Human Molecular Genetics, 2010, Vol. 19, No. 11 **2208–2227**
doi:10.1093/hmg/ddq099
Advance Access published on March 4, 2010

Widespread enzymatic correction of CNS tissues by a single intracerebral injection of therapeutic lentiviral vector in leukodystrophy mouse models

Annalisa Lattanzi[1], Margherita Neri[1,2], Claudio Maderna[1], Ilaria di Girolamo[3], Sabata Martino[3], Aldo Orlacchio[3], Mario Amendola[1], Luigi Naldini[1,2] and Angela Gritti[1,*]

[1]San Raffaele Scientific Institute, Telethon Institute for Gene Therapy (HSR-TIGET), Via Olgettina 58, 20132 Milano, Italy, [2]Vita–Salute San Raffaele University, Via Olgettina 58, 20132 Milano, Italy and [3]Section of Biochemistry and Molecular Biology, Department of Experimental Medicine and Biochemical Sciences, University of Perugia, via del Giochetto, 06126 Perugia, Italy

Received December 30, 2009; Revised and Accepted March 1, 2010

Leukodystrophies are rare diseases caused by defects in the genes coding for lysosomal enzymes that degrade several glycosphingolipids. Gene therapy for leukodystrophies requires efficient distribution of the missing enzymes in CNS tissues to prevent demyelination and neurodegeneration. In this work, we targeted the external capsule (EC), a white matter region enriched in neuronal projections, with the aim of obtaining maximal protein distribution from a single injection site. We used bidirectional (bd) lentiviral vectors (LV) (bdLV) to ensure coordinate expression of a therapeutic gene (β-galactocerebrosidase, GALC; arylsulfatase A, ARSA) and of a reporter gene, thus monitoring simultaneously transgene distribution and enzyme reconstitution. A single EC injection of bdLV.GALC in early symptomatic twitcher mice (a murine model of globoid cell leukodystrophy) resulted in rapid and robust expression of a functional GALC protein in the telencephalon, cerebellum, brainstem and spinal cord. This led to global rescue of enzymatic activity, significant reduction of tissue storage and decrease of activated astroglia and microglia. Widespread protein distribution and complete metabolic correction were also observed after EC injection of bdLV.ARSA in a mouse model of metachromatic leukodystrophy. Our data indicated axonal transport, distribution through cerebrospinal fluid flow and cross-correction as the mechanisms contributing to widespread bioavailability of GALC and ARSA proteins in CNS tissues. LV-mediated gene delivery of lysosomal enzymes by targeting highly interconnected CNS regions is a potentially effective strategy that, combined with a treatment able to target the PNS and peripheral organs, may provide significant therapeutic benefit to patients affected by leukodystrophies.

INTRODUCTION

Lysosomal storage diseases (LSD) are inherited metabolic disorders caused by deficient activity of a single lysosomal enzyme (1). Globoid cell leukodystrophy (GLD) and metachromatic leukodystrophy (MLD) are caused by the deficiency of β-galactocerebrosidase (β-D-galactosyl-*N*-acylsphingosine galactohydrolase, GALC; EC 3.2.1.46) (2) and arylsulfatase A (ARSA; EC 3.1.6.8) (3), respectively. They manifest with a visceral component coupled with a severe and progressive central and peripheral demyelination. Although approaches such as bone marrow and hematopoietic stem cell transplantation (HSCT) or enzyme replacement therapy (ERT) can treat the systemic disease associated with leukodystrophies, the CNS remains a major challenge. An effective therapy requires rapid and robust production coupled with efficient delivery of the deficient enzyme in the whole brain and spinal cord, to prevent demyelination and neuronal damage and to act faster than the disease progression.

Gene therapy represents a promising approach for the treatment of the CNS pathology in LSD, as it has the potential to provide a permanent source of the deficient enzyme (4).

*To whom correspondence should be addressed. Tel: +39 02 2643 4623; Fax: +39 02 2643 4668; Email: gritti.angela@hsr.it

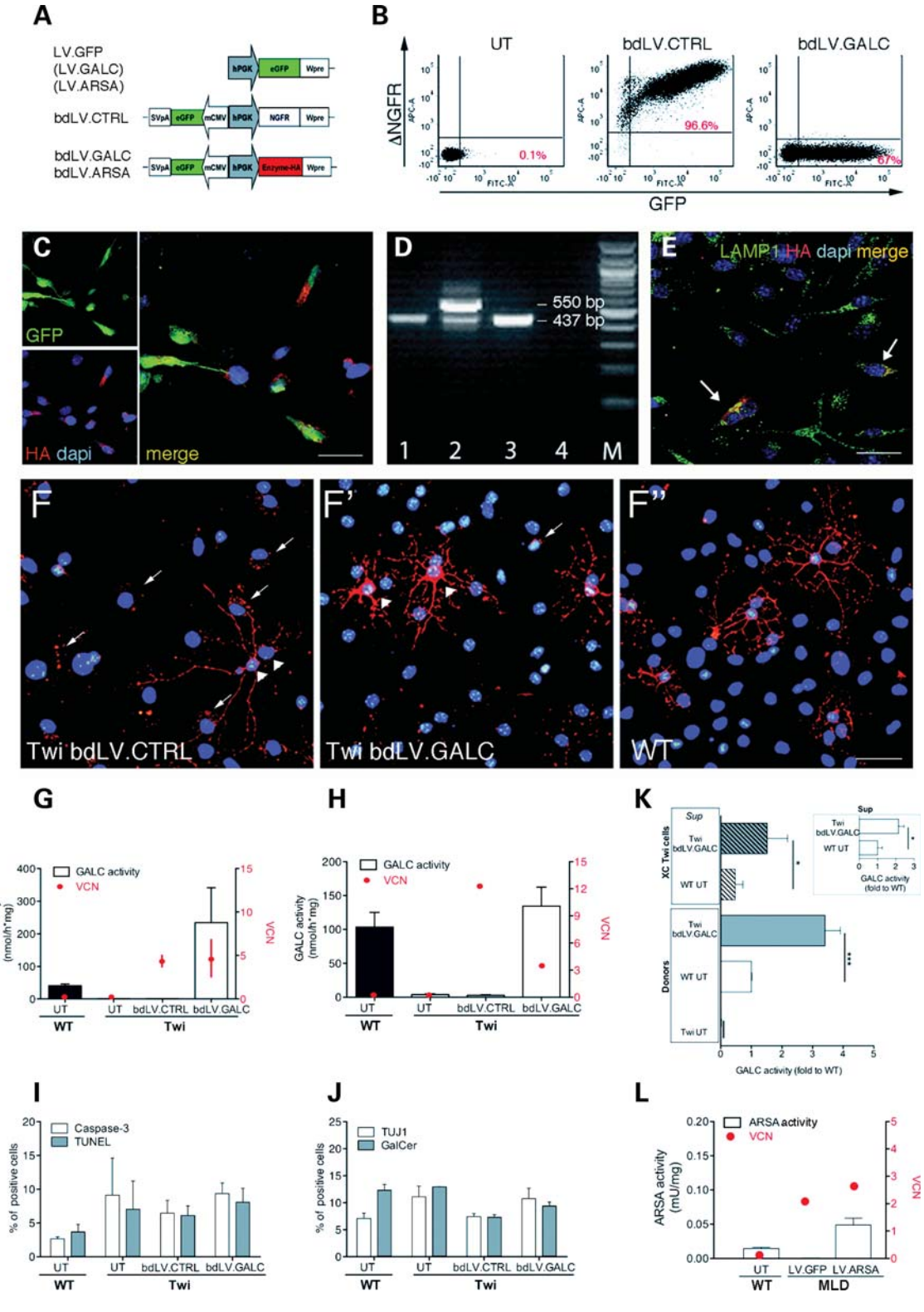

Figure 1. Expression and secretion of functional LV-encoded enzymes *in vitro*. (**A**) Schematic of the monocistronic (LV.GFP, LV.GALC, LV.ARSA) and bidirectional (bd) LV (bdLV.CTRL, bdLV.GALC or bdLV.ARSA) used to transduce NSC *in vitro* and for intracerebral injections. FACS (**B**) and immunofluorescence analysis (**C**) using anti-GFP, anti-NGFR and anti-HA antibodies showed robust bdLV-mediated transduction in Twi NSC and simultaneous expression of the two transgenes in bdLV.GALC-transduced NSC (C). (**D**) Endogenous (437 bp) and vector-encoded GALC mRNA (550 bp) visualized by RT–PCR (see Materials and Methods) in WT and Twi-derived NSC (lane 1 and lane 2: UT and bdLV.GALC-transduced Twi NSC; lane 3: WT NSC; M: marker). (**E**) Merged confocal picture showing co-localization of HA (red) and LAMP1 (green) in LV-transduced Twi NSC. Nuclei counterstained with DAPI. Scale bars, 50 μm. (**F** and **F″**) The anti-galactocerebroside antibody (GalCer, red) specifically identifies oligodendrocytes but also detects intracellular storage in

Intracerebral gene delivery may achieve long-term protein expression and therapeutic benefits in several small and large animal models of LSD, including GM1- and GM2-gangliosidosis (5–8), alpha-mannosidosis (9), mucopolisaccaridosis (10–13), neuronal ceroid lipofuscinosis (14), Niemann–Pick A (15) and leukodystrophies (16–20). The technical and biological challenges underlying the use of gene therapy to target the CNS have been addressed by improving vector design and using novel delivery strategies. Adeno-associated viruses (AAV) exhibit a number of properties that have made this vector system an interesting choice for CNS gene therapy (10,20–22). Similarly, lentiviruses (LV) can mediate robust gene transfer and stable long-term transgene expression into neural cells *in vitro* and *in vivo* without compromising normal cellular functions (23,24). They induce no significant immune responses after delivery into the nervous system (25,26). Also, manufacturing and safety testing for clinical applications have been constantly improved over the past years (27–29).

Lysosomal enzymes are transported along fibers (10,30). Also, they are secreted in the extracellular space, recaptured by the producer cells or by surrounding enzyme-deficient cells and sorted to lysosomes via the mannose-6-phosphate receptor (M6PR) pathway, leading to cross-correction of the metabolic defect (6,31,32). Owing to these peculiar mechanisms, fewer cells can be transduced, reducing the delivery challenge. However, the widespread enzyme distribution required by diseases in which pathology spreads through the nervous system, especially in the brains of large animals and (in a clinical perspective) of human patients, currently requires multiple injections (9,20,33,34), thus increasing the invasiveness of the procedure and the potential adverse effects (26,35).

Given our interest in developing a minimally invasive LV-mediated gene therapy approach to treat leukodystrophies, we targeted the brain external capsule (EC), a white matter region enriched in ascending and descending neuronal projections, with the aim of obtaining maximal protein distribution from a single injection site. The use of bidirectional LV (bdLV) (36) ensured robust gene transfer and stable transgene expression in neural cells and tissues, allowing to monitor simultaneously transgene distribution and enzyme reconstitution in CNS tissues.

A single bdLV injection in the EC of early symptomatic twitcher (Twi) mice, a model of GLD that recapitulates the severity and the rapid progression of the human pathology (37,38), resulted in robust expression and widespread distribution in multiple CNS tissues of a vector-encoded GALC protein displaying the biochemical and functional features of the native WT protein. Similar results were obtained by applying the same approach in a murine MLD model. Our data provide evidence that the sustained protein distribution obtained by targeting a highly interconnected system is enhanced by protein transport through the cerebrospinal fluid (CSF) flow and by efficient cross-correction. Concurrence of these mechanisms results in global enzymatic correction and clearance of tissue storage in the whole CNS, including the caudal most regions (i.e. cerebellum, brainstem, spinal cord), which are severely affected by the pathology but that are not easily corrected by the current available therapeutic approaches.

RESULTS

Expression and secretion of functional GALC and ARSA *in vitro*

We tested the safety and efficacy of the bdLV designed for our *in vivo* study (bdLV.ΔNGFR.GFP, bdLV.GALC-HA.GFP and bdLV.ARSA-HA.GFP; hereon referred to as bdLV.CTRL, bdLV.GALC and bdLV.ARSA, respectively) on neural stem/progenitor cells (NSC) (39) isolated from the subventricular zone (SVZ) of post-natal day 2 (PND2) Twi mice, PND30 MLD mice and age-matched WT littermates. Undifferentiated NSC were transduced with bdLV or monocistronic LV as a control (Fig. 1A). Titers of vector stock ranged between 2×10^9 and 5×10^9 transducing unit (TU)/ml, with particle infectivity $>10^4$TU/ng p24 of vector. All vectors used to transduce cells were matched by titer (3×10^7TU/ml). The number of vector copies per genome (VCN) and the presence of vector-encoded mRNA and proteins were evaluated on NSC after five subculturing passages (>20 days) post-transduction. We proved efficient bdLV.GALC-mediated transduction in NSC (60–90% transduced cells) and simultaneous expression of the two transgenes (Fig. 1B and C). By RT–PCR, we could distinguish the vector encoded from the endogenous GALC mRNA (Fig. 1D), which is present in both WT and Twi-untreated cells (40). The GALC-HA enzyme was expressed in lysosomes, as indicated by LAMP1 co-staining (Fig. 1E) and was functional, as indicated by clearance of intracellular galactocerebroside (GalCer) storage in NSC progeny (Fig. 1F–F″). Not only GALC activity was reconstituted in bdLV.GALC-transduced Twi NSC, but it reached supraphysiological levels (from 2- to 6-fold the WT levels) (Fig. 1G). The functional properties (cell survival, proliferation and differentiation in neurons and glial cells) of GALC overexpressing NSC were not impaired compared with bdLV.CTRL-treated and -untreated WT cells (data not shown). Of importance, similar results in terms of efficacy and safety were obtained following bdLV transduction of Twi NSC-derived differentiated progeny (Fig. 1H–J), an

the differentiated progeny of bdLV.CTRL-treated Twi NSC (F′, arrows). Normal oligodendrocyte morphology and little storage (F′, arrow) were present in the differentiated progeny of bdLV.GALC-treated Twi NSC, similar to what observed in WT cultures (F″). The green channel (GFP direct fluorescence) is not shown. Nuclei were counterstained with DAPI (blue). Scale bars, 50 μm. (**G** and **H**) GALC activity (bars) and VCN (red filled circles) after bdLV transduction of Twi NSC (G) and Twi NSC-derived differentiated progeny (H). (**I** and **J**) bdLV-mediated transduction of Twi NSC-derived differentiated progeny did not increase the basal levels of apoptosis (I; Caspase-3, TUNEL) and did not affect NSC multilineage potential (J; TUJ1, neurons; GalCer, oligodendrocytes). (**K**) Higher levels of intracellular GALC activity in gene-corrected Twi NSC (Twi bdLV.GALC) with respect to WT untreated (UT) cultures (donors) are accompanied by increased levels of GALC in the supernatant (inset). This correlates with more efficient cross-correction (XC) and complete rescue of GALC activity to WT levels in Twi NSC progeny after 72 h exposure to the Sup collected from the differentiated progeny of Twi bdLV.GALC with respect to those exposed to WT sup (XC Twi cells; striped columns). (**L**) Supra-physiological levels of ARSA activity (bars) in LV-transduced MLD NSC. Red filled circles indicate VCN. $^*P < 0.05$, $^{**}P < 0.01$, $^{***}P < 0.001$. One-way ANOVA followed by Bonferroni post-tests or Student's *t*-test (data in the inset).

experimental paradigm that more closely mimics the transduction of brain tissue *in vivo*. Higher GALC activity in the progeny of gene-corrected NSC compared with the WT counterpart (Fig. 1K) correlated with more efficient transfer of the enzyme to untransduced (UT) Twi NSC progeny, which showed higher levels of cross-correction, likely due to the higher fraction of GALC enzyme secreted in the supernatant of GALC overexpressing cells (Fig. 1K, inset).

Similar results in terms of efficacy of transduction and enzyme reconstitution/overexpression were observed following transduction of MLD NSC with LV.ARSA (Fig. 1L). No significant differences in the efficacy and feasibility of transduction between bdLV and monocistronic LV were observed (data not shown).

These results showed that bdLV-mediated transduction of Twi and MLD NSC and progeny is well tolerated and results in efficient and stable enzyme overexpression and secretion, clearance of storage and sustained cross-correction. These results suggested that intracerebral injection of bdLV might result in safe and efficient gene-correction of CNS neurons and glial cells in leukodystrophy mouse models.

Robust cell transduction and stable transgene expression after bdLV.GALC injection in the EC of Twi mice

Affected Twi mice are apparently normal at birth but develop a generalized tremor at about 3 weeks of age followed by progressive weakness and wasting. The disease is fatal by 20–25 days from the onset of symptoms. A cohort of PND21 (early symptomatic) Twi mice and age-matched WT littermates were injected with the CTRL and the therapeutic bdLV. Purified, concentrated vector stock (1 and 1.3 μl of bdLV.CTRL and bd.LV.GALC, respectively, in order to have 2×10^6 total TU) were slowly injected under stereotactic guidance into the left EC (Fig. 2A). Mice were examined 3 weeks after injection (PND42) by immunohistochemical, molecular and biochemical assays to detect the presence of transduced cells, the expression pattern of the transgenes and the enzyme activity within the brain. Indirect immunofluroscence assay followed by confocal analysis showed relevant numbers of GFP^+ cells within and around the injection site (Fig. 2A′). GFP^+ cells were found in about 72 consecutive tissue sections per brain (up to 1 mm rostral and 2 mm caudal to the injection site). The transduction efficiency was 19.61 ± 3.10, 22.28 ± 2.24 and $20.88 \pm 4.85\%$ [average ± standard error of the mean (SE)] in Twi bdLV.CTRL-, Twi bdLV.GALC- and WT bdLV.CTRL-treated animals, respectively (a total of 2855, 3473 and 595 nuclei were counted, respectively), based on GFP^+ and 4′,6-diamidino-2-phenylindole (DAPI) (nuclei) co-staining assessed in serial tissue slices encompassing the injection area. These percentages, which can be slightly underestimated by the fact that only GFP^+ cells with well-defined nuclei in the section were counted, indicated similar transduction efficiency of the two bdLV in this CNS region. A 3D reconstruction (41) using GFP-labeled serial rostro-caudal sections of a representative bdLV.GALC-injected brain revealed that the volume covered by transduced (GFP^+) cells is $\sim 1\ mm^3$ (Fig. 2B), with an average area of $0.61 \pm 0.10\ mm^2$ in sections with the maximal GFP^+ cell density ($n = 3$ sections of the series).

Sections comprising the injection area were stained for Iba-1 (microglia, macrophages), GFAP (astrocytes) and CD3 (T cells), in order to assess the occurrence of an inflammatory response and the presence of infiltrating immune cells. A moderate increase of GFAP and, to a lesser extent, Iba-1 staining was observed at the injection site with respect to the non-injected controlateral hemisphere (Supplementary Material. Fig. S1). CD3 staining was almost undetectable in both hemispheres, in WT and Twi injected mice (data not shown). These results indicate that bdLV injection at the dose tested does not result in overt increased inflammation or T cell-mediated immune response.

GFP^+ cells at the injection site presented with variable morphology (Fig. 2C and D). Double-labeling immunofluorescence using lineage-specific markers followed by confocal analysis showed that $41.74 \pm 4.19\%$ of the GFP^+ cells in bdLV-treated Twi mice were astrocytes (GFAP; Fig. 2E), $15.12 \pm 3.84\%$ were neurons (NeuN; Fig. 2F) and $7.81 \pm 1.46\%$ co-stained with the oligodendroglial marker GST-π (Fig. 2G). Higher proportions of transduced neurons (∼40%) and healthier morphology of GST-π^+ oligodendrocytes were found in WT mice, suggesting that both cell types are affected by the pathologic GLD environment. We did not find significant differences in the cell type composition of the GFP^+ population in Twi mice as regard to the bdLV used (Fig. 2H).

By indirect immunofluorescence followed by confocal analysis using antibodies against the HA peptide or against the GALC protein (42), we detected co-expression of GALC and HA in $79.8 \pm 7.3\%$ of the GFP^+ cells around the injection site (Fig. 2I) in Twi mice injected with bdLV.GALC. We did not detect GALC or HA expression in bdLV.CTRL-treated Twi mice, as expected. GALC immunoreactivity was hardly detectable in untreated and bdLV.CTRL-treated WT mice (data not shown), suggesting low sensitivity of the antibody and indicating that the normal expression level of this lysosomal enzyme in CNS tissues in physiological conditions is lower than that observed after gene transfer. Co-localization of HA and Lamp1 indicated lysosomal localization of the bdLV-encoded GALC (Fig. 2J and J′).

Interestingly, we found a population of $GALC^+GFP^-$ cells (as detected by GALC immunoreactivity) surrounding and intermixed with GFP^+GALC^+ cells (Fig. 2K and L). This suggested that the GALC protein produced by the transduced (GFP^+) cells was secreted in the extracellular space and recaptured by non-transduced (GFP^-) cells, which became metabolic cross-corrected. Quantitative analysis of the cell type composition within the $GALC^+$ cell population (including GFP^+ and GFP^- cells) revealed that neurons were the most represented cross-corrected cells (∼70%, NeuN; Fig. 2K and M), followed by oligodendrocytes (∼25%, GST-π; Fig. 2L and N) and astrocytes (∼6%, GFAP; Fig. 2M).

Distribution of bdLV-encoded proteins after EC injection

Immunofluorescence analysis on serial brain sections from bdLV-injected mice revealed a dense network of GFP^+ fibers spreading rostral (up the olfactory bulb—OB) and caudal (up to the posterior most aspect of the hippocampus) with respect to the injection site, encompassing almost the entire anterior-to-posterior extent of the EC and the posterior internal capsule (Fig. 3A and B).

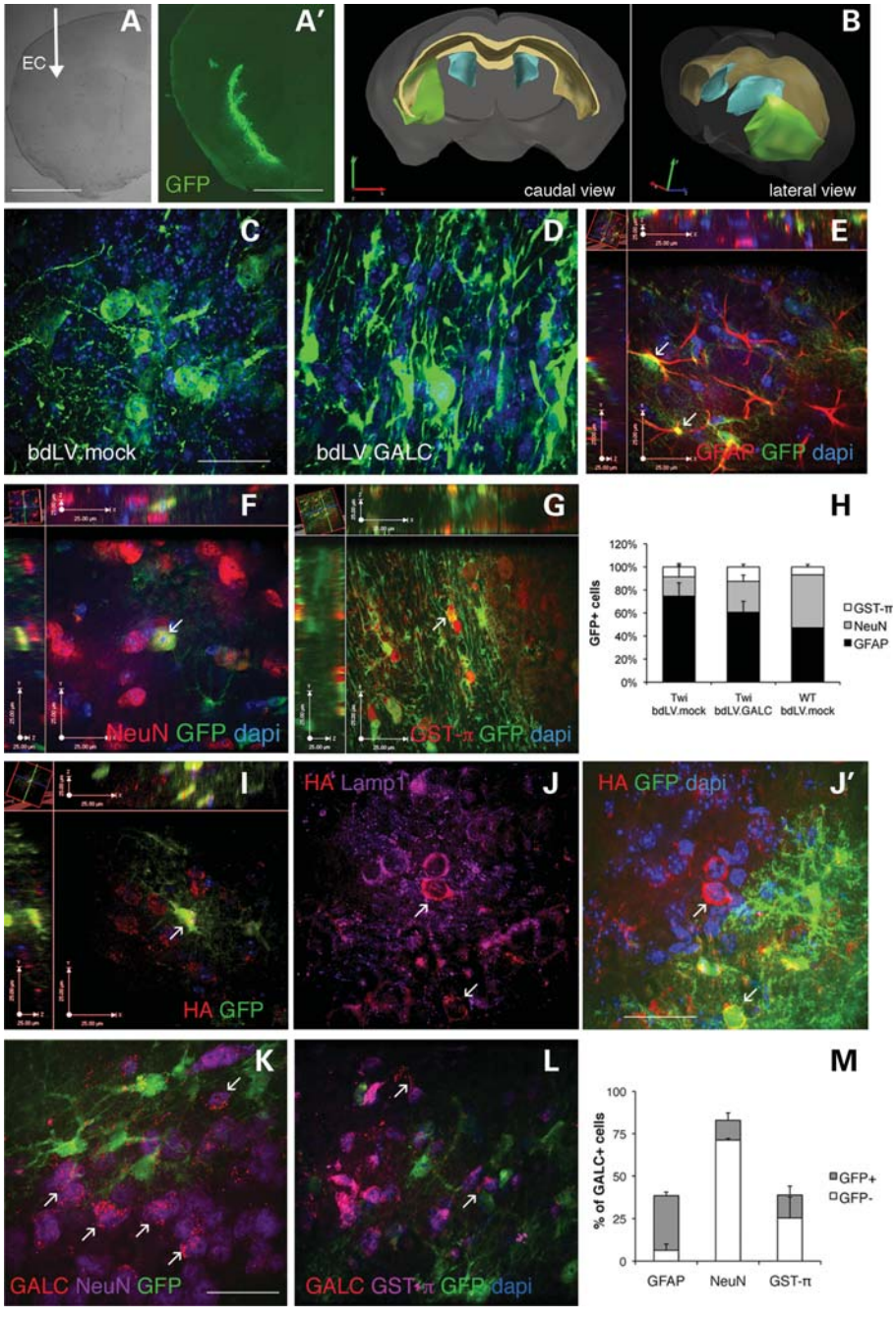

Figure 2. Robust transduction, transgene expression and cross-correction at the injection site. (**A**) Low-magnification (×0.75) bright-field picture of a cresyl-violet counterstained coronal brain section showing the injection site (EC, arrow). (**A′**) Distribution of GFP^+ cells at the site of injection 3 weeks after bdLV injection. Individual confocal pictures (×10 magnification, 64 pictures for each channel) were composed using the Photomerge tool of Adobe Photoshop CS3. Scale bars: 1.5 mm (A), 0.75 mm (A′). (**B**) 3D reconstruction of the forebrain (gray), lateral ventricles (light bue), white matter (light yellow) and GFP^+-transduced tissue (green) of the brain of a representative bdLV.GALC-treated mouse at 20 days post-injection. Reconstruction was obtained from sequential sections analyzed for stereology using the Neurolucida software, which returned the enclosed volumes for each region: forebrain, 114.33 mm^3; lateral ventricles, 0.455 mm^3; white matter, 4.65 mm^3; GFP^+ tissue, 0.99 mm^3. (**C** and **D**) Higher magnification confocal pictures taken at the injection site of bdLV.CTRL (C) and bdLV.GALC-injected (D) Twi mice showed GFP^+ cells with variable morphology. Green, GFP; nuclei counterstained with DAPI (blue). (**E**–**G**) Representative confocal pictures after Z-stack analysis showing GFP^+ cells (green) expressing markers of astrocytes (E; GFAP), neurons (F; NeuN) and oligodendrocytes (G; GST-π). Arrows and yellow-orange color indicate co-localization of signal. Scale bars: 30 μm (C–G, shown in C). (**H**) 100% stacked column chart showing percentages of neurons (NeuN), astrocytes (GFAP) and oligodendrocytes (GST-π) within the GFP^+ cell population in bdLV-injected Twi and WT mice. (**I**) Representative confocal picture after Z-stack analysis shows GFP (green) and HA (red) co-expression (arrows and yellow-orange color). Note the presence of surrounding HA^+GFP^- cells. (**J** and **J′**) Co-localization of HA (red) and Lamp1 (violet) in GFP^+ cells (green) indicates lysosomal localization of the bdLV-encoded GALC. Nuclei counterstained with DAPI (blue in J′). Scale bars: 30 μm (shown in J). (**K** and **L**) Representative confocal pictures showing GFP^- $GALC^+$ cells (cross-corrected cells; red) expressing markers of neurons (K; NeuN, violet) and oligodendrocytes (L; GST-π, violet). GFP, green; nuclei counterstained with DAPI (blue). Scale bars: 30 μm (shown in K). (**M**) Chart showing the cell type composition of GFP^+ and GFP^- cells within the $GALC^+$ cell population (assessed as $GALC^+$ cells on the total number of nuclei) at the injection site of bdLV.GALC-treated mice.

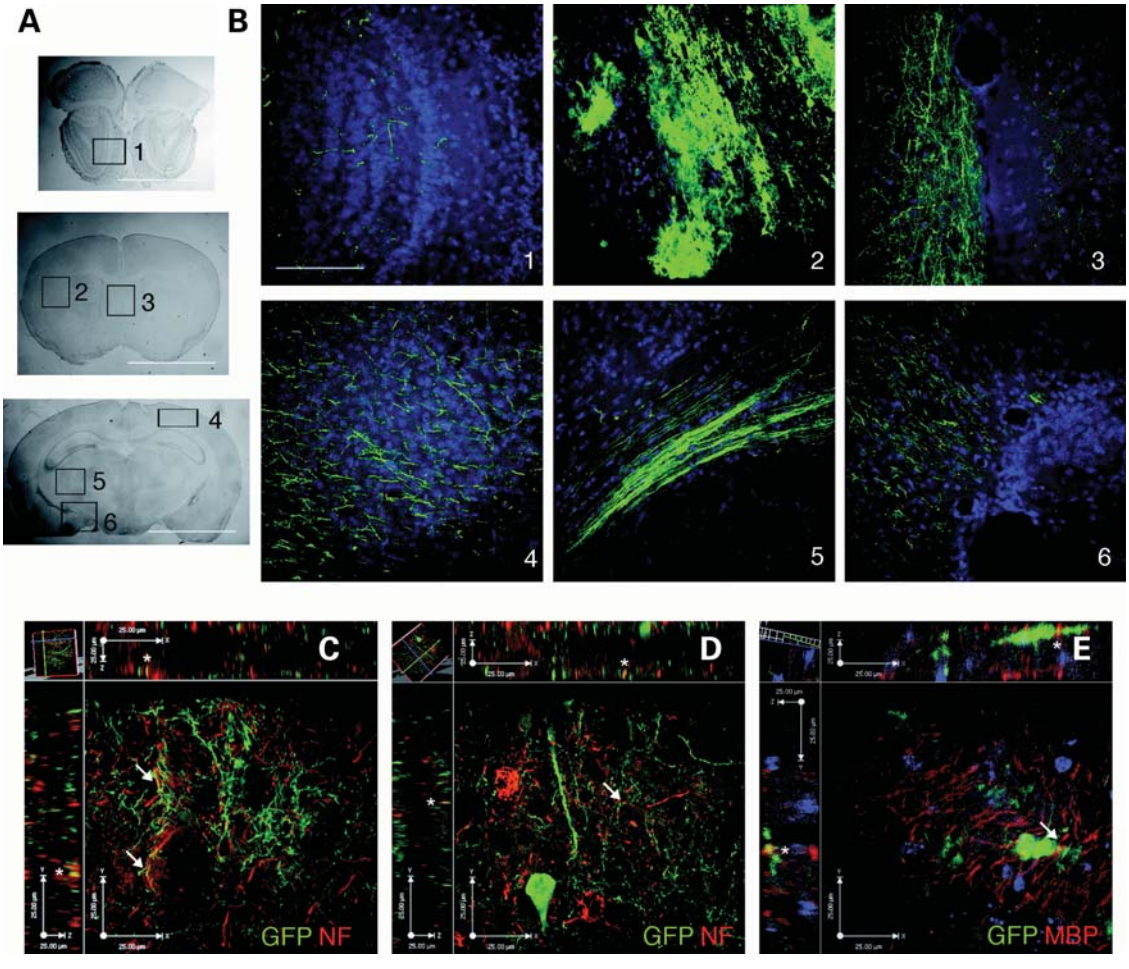

Figure 3. Transport of the GFP protein in CNS regions far from the injection site. (**A**) Serial rostro-caudal brain sections from bdLV.CTRL-injected mice were processed for immunofluorescence analysis using an anti-GFP antibody. Scale bars: 3 mm. (**B**) Representative pictures (1 to 6) of the brain regions indicated by boxes and matched numbers in A. A dense network of GFP^+ fibers spread from the injection site (2), rostral up to the OB (1) and caudally in the injected and in the non-injected controlateral hemisphere (3), reaching the cortex (4), down to the posterior most aspect of the hippocampal area and the posterior internal capsule (5 and 6). Scale bars: 500 μm (1 to 6, shown in 1). (**C**–**E**) Confocal Z-stack images showing the presence of GFP^+ projections (green) co-stained with a pan-NF marker (SMI-311, red; C, D) or with myelin basic protein (MBP, red; E). Co-localization is shown by arrows in the xy plane and by asterisks in the xz and yz planes.

Although the majority of the GFP^+ projections were found in the injected hemisphere, a relevant number was also observed in the controlateral hemisphere, thus suggesting protein transport along projections, mainly in the white matter tracts (Fig. 3B). However, we detected only few GFP^+ projections co-labeled with a pan-neurofilament (NF) marker (Fig. 3C and D) or with myelin basic protein (MBP; Fig. 3E). Only scattered GFP^+ projections were observed in the brainstem, cerebellum and spinal cord. A similar pattern of GFP distribution and expression was found after EC injection of a monocistronic LV.GFP vector (Supplementary Material, Fig. S2).

We could not detect GALC or HA expression by IF analysis in areas far from the injection site, consistent with the expected lysosomal distribution of the enzyme, which is restricted to the perinuclear region. In order to have more conclusive documentation of enzyme spreading, we resorted to biochemical assays. The whole brain and the spinal cord were isolated from PND42 bdLV.CTRL- and bdLV.GALC-injected Twi mice as well as from age-matched untreated WT and Twi controls. The brains were cut in five consecutive slices comprising the following regions (rostral to caudal): OB; anterior telencephalon (aTel, comprising the injection site), posterior telencephalon (pTel), pons/medulla (Pons) and cerebellum (Cb). Tissue from each slice was then divided along the midline in order to separate the injected (left) from the controlateral (right) hemisphere. The total spinal cord (SC; cervical + thoracic + lumbar) was collected (Fig. 4A). The presence of bdLV-encoded GALC protein was initially investigated by western blot (WB) analysis using an anti-HA antibody after immunomagnetic enrichment of the HA-tagged GALC from total tissue lysates. This assay revealed a band of ~80 kDa, the expected molecular weight (MW) of one of the GALC forms, in tissues from bdLV.GALC-treated brains. This band was absent from bdLV.CTRL-treated controls (Fig. 4B). In order to compare levels of GALC expression in gene therapy-treated mice with those found in WT tissues, we then assayed directly protein expression on tissue extracts using the GALC antibody. Remarkably, WB

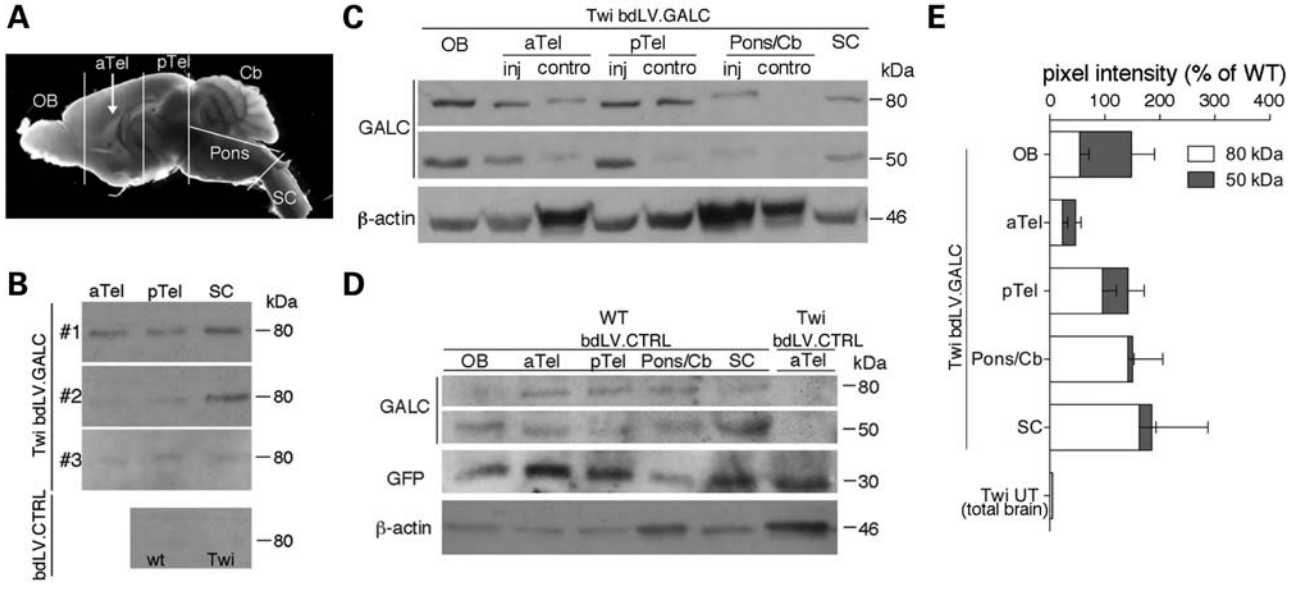

Figure 4. Widespread distribution of GFP and GALC proteins in CNS tissues of bdLV-injected mice. (**A**) Schematic of brain and spinal cord dissection in bdLV.CTRL- and bdLV.GALC-injected Twi mice and from age-matched untreated (UT) WT and Twi controls. The arrow indicates the injection site (see also Results). Contro, controlateral non-injected hemisphere. (**B**) WB analysis using an anti-HA antibody after immunomagnetic enrichment of the HA-tagged GALC from total tissue lysates revealed a band of about 80 kDa in aTel, pTel and SC tissues from bdLV.GALC-treated mice (#1, #2 and #3 represent tissues from different mice) that was absent from bdLV.CTRL-treated WT or Twi controls. (**C** and **D**) WB using the anti-GALC antibody revealed bands of 80 and 50 kDa in tissues from all the CNS regions of bdLV.GALC-treated Twi mice (C). These bands were undetectable in tissues derived from bdLV.CTRL-treated Twi mice (D). The GFP protein was detected in tissues from WT and Twi mice injected with bdLV.CTRL (C and D). β-Actin was used as normalizer. (**E**) Densitometry of WB bands (see Materials and Methods) confirmed the complete rescue of GALC expression in all the CNS regions of bdLV.GALC-injected mice.

analysis revealed bands of the expected MW (80 and 50 kDa) (40) in tissues from all the CNS regions of bdLV.GALC-treated Twi mice (Fig. 4C), with levels of expression similar or even higher to those detected in region-matched tissues from bdLV.CTRL-treated and untreated WT mice (Fig. 4D and E). No bands corresponding to the GALC protein were detected in tissues from bdLV.CTRL-treated Twi mice (Fig. 4D). The GFP protein was detected in CNS tissues from mice injected with bdLV.CTRL (Fig. 4C) and bdLV.GALC (data not shown), as expected.

Global rescue of enzymatic activity in CNS tissues of bdLV.GALC-treated Twi mice

In order to assess whether the widespread GALC distribution observed in CNS tissues of bdLV.GALC-treated mice led to metabolic correction, we evaluated GALC activity in the five rostro-caudal brain regions isolated from bdLV-injected mice using a biochemical assay which employs the artificial substrate MUGAL in the presence of $AgNO_3$, a specific inhibitor of the β-galactosidase activity (43).

Data showed significant increase of GALC activity in Twi and WT mice treated with the therapeutic vector with respect to untreated (data not shown) and bdLV.CTRL-treated controls (Fig. 5A). At 3 weeks after injection, GALC activity was rescued to 50% of the WT levels in brain regions comprising the injection site and rostral to it (aTel, OB) in bdLV.GALC-treated Twi mice. Importantly, complete enzymatic correction was achieved in brain regions caudal to the injection site (pTel, Pons, Cb). Also, in agreement with data obtained by histochemistry and WB analysis, similar (or even higher) levels of enzymatic activity were measured in the controlateral non-injected hemisphere, all along the rostro-caudal axis. Complete enzymatic correction was observed in spinal cord tissues.

In agreement with results from previous studies (10), bdLV injection in the ventral tegmental area (VTA) resulted in widespread protein distribution in several CNS regions but failed to achieve complete enzymatic correction in the caudal most regions (pons and SC) (data not shown). Striatal injection resulted in limited distribution of the GALC protein and significantly lower levels of GALC activity in all the CNS regions considered (data not shown).

Although the 80 kDa form of the GALC protein (which is intracellularly cleaved into the 50–55 kDa and the 30 kDa fragments) is described to bear catalytic activity *in vitro* (44), the multimeric high MW form (tetramer, hexamer) are thought to be the native functional enzyme in tissues (45). In order to check whether the rescue of GALC activity observed in CNS tissues of bdLV.GALC-treated animals was due to the ability of the transgenic GALC protein to assemble in the multimeric functional form, we performed gel-filtration on sephadex S300-chromatography analysis. The chromatographic profile of WT CNS tissues (aTel and SC are shown in Fig. 5B) revealed a peak of activity (600–700 kDa) corresponding to the GALC enzyme, as demonstrated by measuring the enzymatic activity using the specific GALC assay (Fig. 5B). This peak of activity was absent in Twi tissue but was restored to 60–75% of WT levels in CNS tissues from bdLV.GALC-treated mice. These results indicate that the transgenic GALC protein shows biochemical features indistinguishable from those of the WT native enzyme.

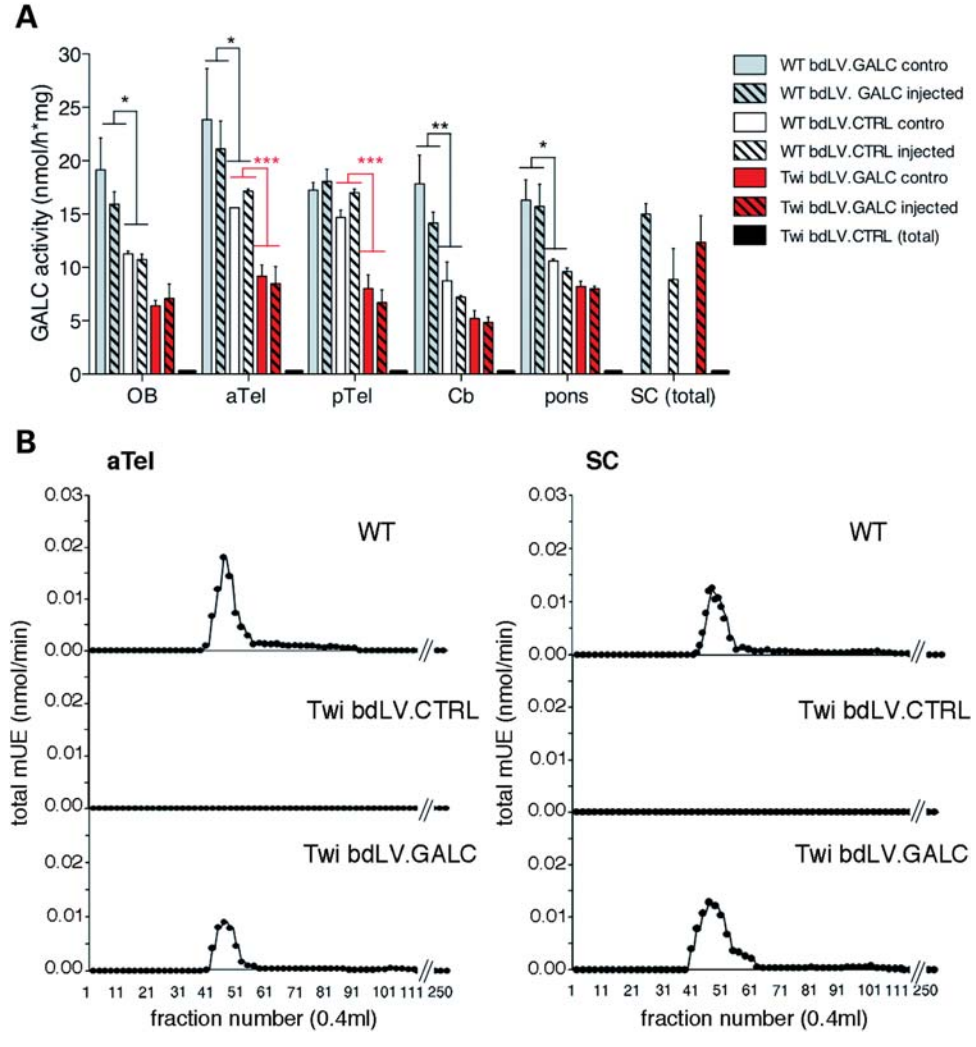

Figure 5. Enzymatic reconstitution in CNS tissues of bdLV.GALC-treated mice. (**A**) Increased GALC activity was measured in bdLV.GALC-treated WT mice (gray columns) with respect to bdLV.CTRL-treated mice (white columns) in almost all CNS regions. In bdLV.GALC-treated Twi mice (red columns), GALC activity was rescued to 50% of the WT levels in brain regions comprising the injection site and rostral to it (aTel, OB). Complete enzymatic correction was achieved in brain regions caudal to the injection site (pTel, Pons, Cb). Similar levels of enzymatic activity were measured in the controlateral (contro) non-injected hemisphere (red striped columns). GALC activity was undetectable in bdLV.CTRL-treated Twi mice (black columns). $^{*}P < 0.05$, $^{**}P < 0.01$,$^{***}P < 0.001$. Two-way ANOVA followed by Bonferroni post-test (since no significant differences were found between GALC levels in the injected and controlateral hemispheres for each CNS region, these values were averaged in this analysis). (**B**) Gel-filtration on Sephadex S300-chromatography analysis on representative CNS tissues (aTel controlateral and SC) from untreated WT, bdLV.CTRL- and bdLV.GALC-treated Twi mice. The peak of activity (600–700 kDa) corresponding to GALC enzyme, as demonstrated by measuring GALC activity, was absent in bdLV.CTRL Twi tissues but was restored to 60–75% (measured as the area under the peak) of the WT levels in CNS tissues from bdLV.GALC-treated Twi mice.

In order to further validate the efficacy of a single EC injection in achieving widespread distribution of a lysosomal enzyme in a different LSD model, we injected bdLV.ARSA in 6-month-old $As2^{-/-}$ mice, which serve as a murine model of MLD (46). Analysis performed 3 weeks after injection showed GFP expression ($16.0 \pm 1.2\%$ GFP^{+} cells on the total nuclei; 1838 nuclei counted; Fig. 6A and B) and the presence of integrated bdLV genome (VCN $= 0.67 \pm 0.2$) at the injection site (aTel region), confirming efficient bdLV.ARSA-mediated transduction. More than 90% of transduced (GFP^{+}) cells at the injection site co-expressed HA, and the population of cross-corrected ($GFP^{-}HA^{+}$) cells was consistently detected (Fig. 6C). Immunofluorescence analysis documented rapid and widespread rostro-caudal GFP distribution in bdLV.ARSA-injected mice (Fig. 6D). Remarkably, ARSA activity was completely restored to WT levels in all the brain regions (in both the injected and in the controlateral hemispheres) and spinal cord of bdLV.ARSA-injected mice (Fig. 6E and F). These results demonstrated that bdLV.ARSA injection in the adult EC is effective in achieving complete metabolic correction in the brain and spinal cord tissues of MLD mice and strongly validate the efficacy of this gene delivery approach to correct enzymatic CNS deficiency in leukodystrophies.

Mechanisms of enzyme distribution in CNS tissues

The presence of the bdLV-encoded enzymes in multiple CNS regions, rostral and caudal to the injection site, in the injected

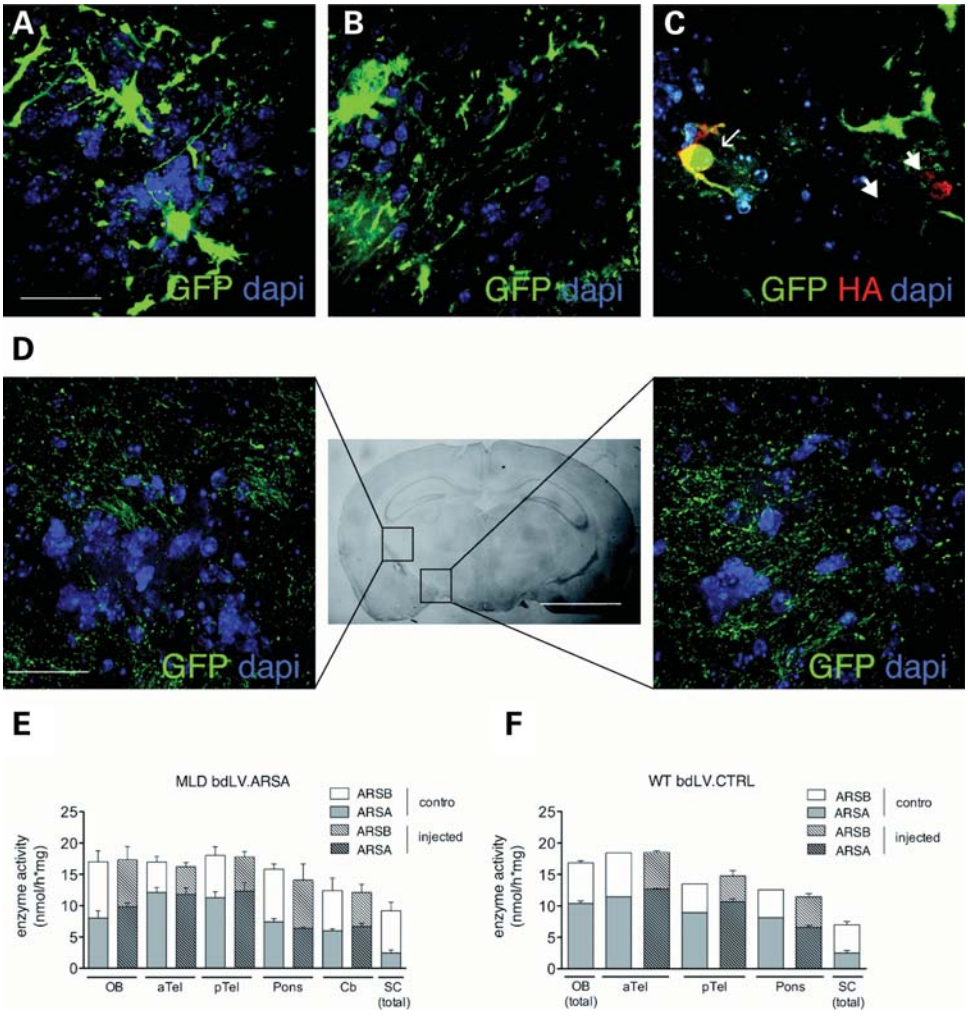

Figure 6. Protein distribution and enzymatic reconstitution in CNS tissues of bdLV.ARSA-treated MLD mice. (**A** and **B**) Two representative confocal pictures showing robust transduction and GFP expression at the injection site 3 weeks after injection of bdLV.ARSA. (**C**) Representative picture showing a transduced cell (GFP^+) co-expressing HA (arrow) surrounded by GFP^-HA^+ cells (putative cross-corrected cells; thick arrows). (**D**) Confocal pictures taken at the level of posterior white matter (boxed areas in the low magnification bright-field picture) show a network of GFP^+ fibers. In all panels: green, GFP; red, HA; nuclei counterstained with DAPI (blue). (**E** and **F**) Complete reconstitution of ARSA activity in the injected and controlateral (contro) hemispheres and correct relative proportions between ARSA and ARSB activity were found in CNS tissues from bdLV.ARSA-injected $As2^{-/-}$ mice (MLD LV.ARSA; E) when compared with bdLV.CTRL-treated WT controls (WT LV.CTRL; F). Scale bars: 100 μm (A–D, confocal pictures; shown in A) and 2.5 mm (bright field picture in D).

and non-injected controlateral hemisphere, suggested that both diffusion and axonal transport might contribute to GALC and ARSA distribution, as previously reported for these and other lysosomal enzymes (6,17,32). Release of lysosomal enzymes into the interstitial space and distribution to CNS tissues by CSF flow has also been proposed (6,47–52). In order to investigate the impact of this mechanism in our experimental approach, we directly measured GALC activity in the CSF collected from the cysterna magna of WT (either untreated or bdLV.CTRL-treated; $n = 5$), Twi bdLV.CTRL- ($n = 3$) and Twi bdLV.GALC-treated mice ($n = 6$) immediately prior to euthanasia. Although GALC activity was undetectable in Twi bdLV.CTRL-treated mice, bdLV.GALC-treated mice showed levels of enzyme activity similar to those measured in WT CSF (Fig. 7A). This result indicated CSF flow as an important mechanism contributing to the efficient distribution of the GALC enzyme in CNS tissues in our system.

Different from what reported in recent studies using intracerebral AAV injection (6,10) and in agreement with other studies using VSV-G pseudotyped LV, we detected bdLV genome (Fig. 7B) and bdLV-encoded mRNA for GALC, GFP (Fig. 7C) and ARSA (data not shown) only in tissues surrounding the injected site (left aTel). This indicated that, in our experimental approach, the transport of vector particles or vector-encoded mRNA does not contribute to enhance the efficacy of the vector injection in achieving high levels of enzymatic CNS correction.

Effect of enzyme distribution on disease lesions

To determine whether the widespread distribution of GALC enzyme would result in prevention or reversal of lysosomal storage, we analyzed the pattern of lectin histochemistry in the brain and spinal cord of bdLV.CTRL- and bdLV.GALC-treated

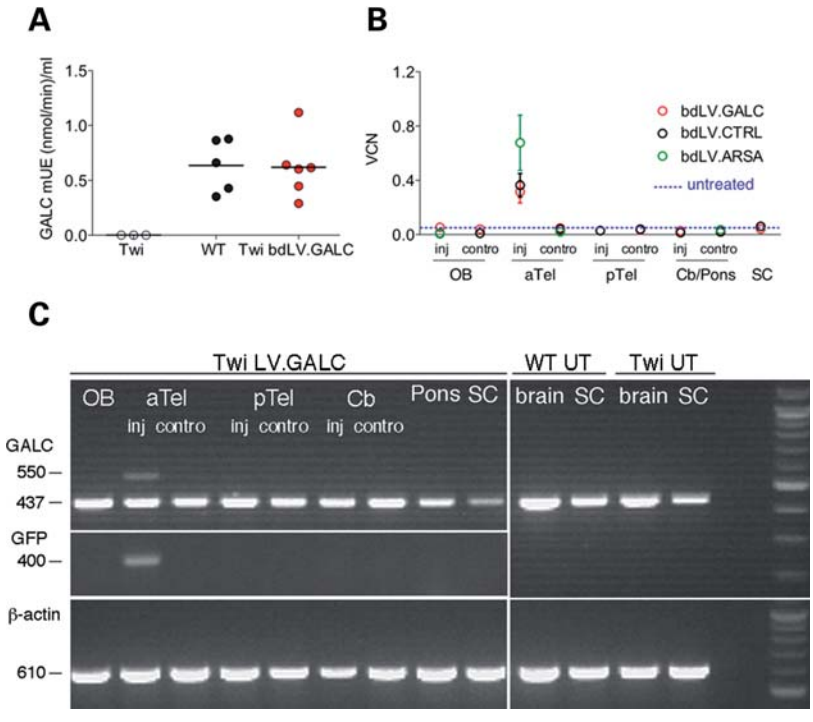

Figure 7. Mechanisms of GALC distribution in CNS tissues. (**A**) bdLV.GALC-treated mice showed levels of GALC activity similar to those measured in WT CSF. GALC activity was undetectable in the CSF of Twi mock-treated mice. (**B**) bdLV genome, assessed by qPCR in bdLV.GALC- and bdLV.ARSA-injected mice, was detected only in tissues comprising the injected region (left aTel). (**C**) RT–PCR using: (i) primers in the GFP coding region and (ii) two pairs of primers designed on a sequence of the bdLV cassette (expected size 550 bp) and on a sequence of the endogenous GALC (expected size 470 bp) revealed bdLV-encoded GFP and GALC mRNA only in the left aTel. β-Actin was used as normalizer.

Twi mice as well as of untreated controls. Lectin staining is considered a useful tool to visualize globoid cells in CNS tissues from murine and dog models of GLD (53,54). Quantification of lectin-immunopositive area on selected CNS regions (CC, Cb, Pons and SC; Fig. 8A) indicated a dramatic increase of tissue storage in bdLV.CTRL-treated Twi mice compared with WT littermates. The amount of storage was significantly reduced in all the CNS regions of bdLV.GALC-treated mice (Fig. 8B and D). In addition, immunoreactivity for the macrophagic/microglial marker F4/80 was significantly reduced in matched brain regions of these mice, with levels of expression approaching those of WT animals (Fig. 8C and E). Only a moderate reduction of immunoreactivity for GFAP (astroglia; Fig. 8F) and Iba-1 (microglia; Fig. 8G) was found in bdLV.GALC-treated Twi mice with respect to bdLV.CTRL-treated littermates, although a partial normalization of cell morphology towards the WT phenotype was observed.

Overall, these results support the notion that the vector-encoded GALC enzyme transported in CNS tissues far from the injection is functional and able to partially clear tissue storage, particularly in the macrophagic-derived globoid cell population.

DISCUSSION

We have explored an intracerebral gene therapy approach based on a single LV injection in the brain EC of leukodystrophy mouse models. This approach resulted in rapid, sustained and widespread expression of the functional enzymes in the whole brain and spinal cord, with high-level enzymatic correction and significant reduction of tissue storage. Although the distribution of transduced cells was restricted to a little portion of the injected hemisphere, unprecedented spread of enzyme expression and biochemical correction occurred through (i) robust LV-mediated transduction of neural cell types at the injection site; (ii) efficient production and secretion of the functional proteins by transduced cells; (iii) widespread distribution of bioactive enzymes (GALC and ARSA) in CNS tissues through different mechanisms, including axonal transport, distribution through CSF flow and cross-correction of non-transduced cells.

LV-mediated gene delivery

White matter and myelinating cells play an essential role in brain function and integration between different areas of the CNS. They are the main sites of pathology in leukodystrophies, thus representing important targets for gene therapy strategies aimed at treating these diseases. Use of lentiviral vectors (LV) offers multiple advantages for gene replacement therapy. They combine efficient delivery, capacity to integrate into the host genome to provide stable long-term transgene expression, absence of any viral genes in the vector and absence of interference from pre-existing viral immunity. Results from this and previous studies (55–57) show that LV robustly transduce neurons, astrocytes and oligodendrocytes *in vitro*. In the CNS of adult rodents (23,24,58,59) and

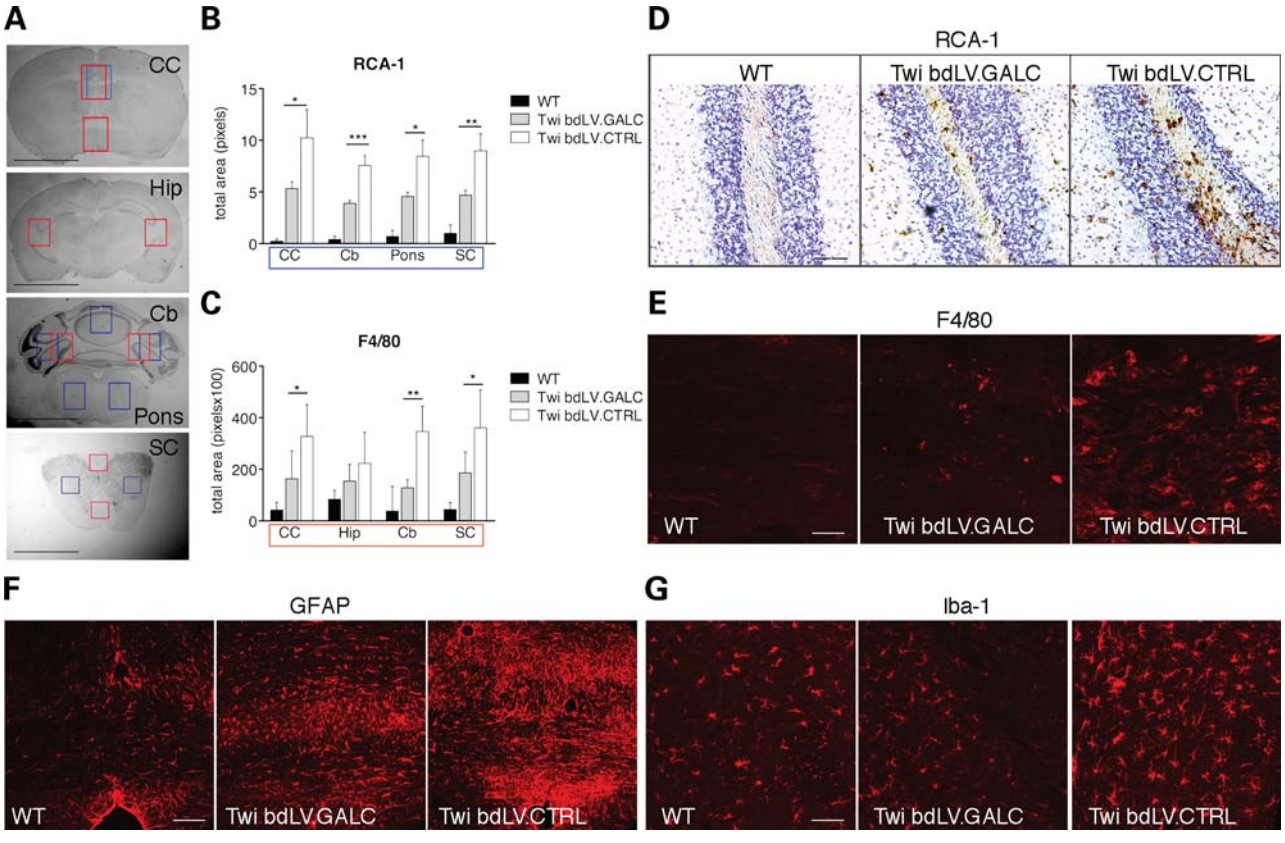

Figure 8. Detection of disease lesions and pathology. Histochemistry using biotinylated lectins (RCA-1; glycolipid storage and globoid cells) and indirect immunofluorescence analysis using anti-F4/80, anti-Iba1 (microphages and microglia) and anti-GFAP (astrocytes) antibodies were performed on selected region-matched rostro-caudal tissue slices (**A**) from bdLV.CTRL- and bdLV.GALC-treated and on untreated WT and Twi mice. Pictures of defined areas in each slice (indicated by blue boxes for RCA-1 and red boxes for the other antigens) were taken, and the total immunopositive area in each picture (expressed in pixels) was calculated using the ImageJ software. Tissue slices in which the primary antibodies were omitted (for Iba1 and GFAP) or tissue slices from untreated WT mice (for F4/80 and RCA-1) were used to set the signal threshold. CC, corpus callosum; Hip, hippocampus; Cb, cerebellum; SC, spinal cord. (**B** and **C**) Quantification of lectin- (B) and F4/80 (C) immunopositive area indicated a dramatic increase of tissue storage (globoid cells) and activated macrophages/microglia in bdLV.CTRL-treated Twi mice when compared with WT littermates that were significantly reduced in all the CNS regions of bdLV.GALC treated mice. (**D** and **E**) Representative pictures showing lectin$^+$ (D; cerebellum) and F4/80$^+$ (E; corpus callosum) cells in WT mice, bdLV.GALC- and bdLV.CTRL-treated Twi mice. (**F** and **G**) A moderate reduction of immunoreactivity for GFAP (astroglia; F) and Iba-1 (microglia; G) was found in bdLV-GALC-treated Twi mice with respect to mock-treated littermates, together with a partial normalization of cell morphology towards the WT phenotype (representative pictures of the corpus callosum are shown). Scale bars: 2 mm (A, CC and Cb/Pons), 2.5 mm (A, Hip), 1.5 mm (A, SC); 250 μm (D, E, F and G). $^*P < 0.05$, $^{**}P < 0.01$, $^{***}P < 0.001$. Two-way ANOVA followed by Bonferroni post-test.

non-human primates (60), neurons are the main cellular target of LV (and especially VSV-G pseudotyped LV), whereas glial cells seem to be transduced to a lower efficiency (17,61–64). In our white matter injection, bdLV efficiently targeted neurons, although we did not observe high percentages of neuronal transduction reported in previous studies describing targeting of gray matter regions. Indeed, our analysis demonstrated robust bdLV-mediated gene transfer in glial cells. Interestingly, the higher proportion of astrocytes in the transduced GFP$^+$ population found in bdLV-injected Twi mice with respect to the WT counterpart mirrors the increased number of astroglial cells that are present in Twi versus WT brains as a consequence of the pathology. Similarly, the small number of transduced oligodendrocytes detected in Twi tissues is likely due to low fitness or to selective death of this cell type at the late stages of the disease more than to inefficient LV transduction in this cell type. The finding that higher numbers of healthy GFP$^+$GST-π$^+$ cells are retrieved in the brain of age-matched WT mice supports this concept.

Our molecular data on the presence of vector genome and vector-encoded mRNA in CNS tissues of bdLV-injected mice are consistent with the notion of moderate LV physical spread from the injection site, either in the gray matter (12,17,65) or along the WM tracts (59). In contrast, a broader diffusion of vector particles or mRNA has been described following injection of several AVV serotypes (i.e. AAV2/1, AAV5, AAV9) in the brain parenchyma (6,10,20).

Enzyme distribution in mouse CNS tissues

The simultaneous and robust expression of the two transgenes ensured by bdLV allowed us to evaluate the efficacy of transduction, to monitor distribution and to visualize transduced versus non-transduced cross-corrected cells. Our *in vitro* data show that transduced NSC-derived glial and neuronal cells express supra-physiological levels of GALC, which, in turn, resulted in more efficient cross-correction of GALC-deficient differentiated neural cells. Consistently, *in vivo*

transduced cells robustly overexpressed GALC compared with WT cells, as shown by immunohistochemistry and by quantification of the total protein output from a limited number of transduced cells. The widespread expression of GFP and either GALC or ARSA in brain regions far from the injection site reflects the high connectivity of the brain region targeted by LV in our study and is consistent with the notion that axonal transport ensures distribution of proteins in the brain (6,7,15,17). In fact, the EC contains axonal fibers running between the cerebral cortex and the pyramids of the medulla, at the lower part of which the majority decussates and passes into the anterior columns of the spinal cord. This likely explains the high expression of transgenic proteins in posterior CNS regions of the controlateral non-injected hemisphere. Thus, bdLV injection in the EC provides benefit in regions that are severely affected in the GLD mouse model and in early-onset forms of leukodystrophies (66,67) but are not easily targeted by the currently available gene therapy approaches.

Lysosomal enzymes are sorted to lysosomes as pro-enzymes through a specific pathway controlled by the insulin-like growth factor-II (IGF-II)/M6PR (68–70). A fraction of the pro-enzyme escapes this pathway (71) and is secreted in the extracellular space, where it can be recaptured by the producer cells or by surrounding cells (via M6PR expressed on the cell membrane) and sorted to lysosomes, leading to cross-correction of the metabolic defect and further spread within the brain (5,31,32). Our results showing that this mechanism is particularly active in neurons are in agreement with previous studies (17,31,32) and might reflect a prevalent neuronal localization of the M6PR. Still, we provide evidence for the presence of cross-corrected oligodendrocytes and, to a lesser extent, astrocytes in the brain of bdLV.GALC-treated mice, suggesting that M6PR-independent uptake of the GALC enzyme might occur in glial cells.

The mechanism of distribution by CSF flow has been proposed for several lysosomal enzymes and might explain the efficacy of intracerebroventricular or intrathecal infusion of vectors (6,47,48,50–52) or purified recombinant enzymes (49,72) in achieving widespread correction of lysosomal storage in the brain. By direct assessment of GALC activity in the CSF, we conclusively demonstrate that the GALC protein is efficiently secreted into the interstitial space and distributed in CNS tissues through the CSF flow. In our system, this mechanism likely prevails over axonal transport in ensuring widespread protein distribution. Of importance, the small population of LV-transduced cells in the Twi brain produce and secrete enough GALC enzyme to ensure CSF levels comparable with those measured in physiological conditions.

The GALC protein is generated as an 80 kDa precursor protein that is processed within lysosomes into the 50 kDa and 30 kDa fragments (73). The precursor protein secreted in the extracellular milieu escapes the processing pathway, still retaining enzymatic activity (44). Our WB analysis revealed the presence of the 80 kDa and 50 kDa forms in CNS tissues of bdLV.GALC-treated animals, which are identical to the apparent MW of endogenous precursor and processed GALC forms detected in brain tissues of WT mice, using the same antibody. This strongly suggests that the LV-encoded enzyme has been properly trafficked to lysosomes (as also indicated by LAMP1 co-labeling), where it is likely to be functional.

Data obtained on partially purified galactocerebrosidases of human placenta, liver and brain indicate that four molecular-weight forms can be resolved by gel filtration and suggest that an aggregation process proceeding from a monomer (precursor protein) to a dimer, and from the dimer to either a tetramer or a hexamer (MW ~750 kDa) takes place in normal tissues, the highest MW form being the most abundant and displaying the highest enzymatic activity (45). The high homology between the human and the murine GALC proteins suggests similar biochemical features but no detailed information was currently available on the active native form of the murine GALC. We demonstrate for the first time that a high MW (likely the hexamer) GALC protein is present in brain tissues of WT mice. Different from what described in human tissues (45), we could not resolve by gel filtration the lower MW forms, possibly because they are present in too low amount compared with the highest MW counterpart. Importantly, our biochemical and molecular analyses together prove that bdLV-encoded GALC is correctly translated and processed inside the cells and it is able to assemble in the multimeric native protein, which can be secreted and transported far from the injection site through different mechanisms, maintaining full enzymatic activity. Our data also indicate that the C-terminal HA tag has no appreciable impact on the activity of LV-encoded GALC and ARSA. In addition, the super imposable pattern of tissue distribution and enzymatic reconstitution measured following EC injection of bdLV.GALC in Twi mice and bdLV.ARSA in MLD mice give proof of principle of the applicability of this gene therapy approach in several LSD with CNS involvement. In this perspective, the efficient delivery of the two genes allowed by bdLV may be useful in gene therapy settings where the simultaneous expression of two proteins is necessary (i.e. the α and β-subunits of the β-hexosaminidase enzyme in Sandhoff disease) or might provide additional therapeutic benefit by enhancing the clearance of tissue storage (i.e. SUlphatase Modifying Factor 1 and specific sulfatases in different models of sulfatase deficiencies) (74).

Biochemical correction versus phenotype rescue: clinical relevance

It is accepted that enzyme activity representing as little as 1–5% of normal levels in the CNS is sufficient to correct storage lesions and to rescue phenotype in experimental animal models of LSD (75,76). However, requirements of up to 50–60% of normal levels have also been indicated (8), likely according to the severity of the disease model and possibly to some disease-specific factors. According to these notions, our gene therapy approach results in complete biochemical correction of the bulk CNS tissue and this correlates with substantial clearance of storage from the macrophage/microglia population, which represents the hallmark of pathology in the severe GLD mouse model. We performed our treatment in early symptomatic Twi mice, in order to better model what can be attempted in the vast majority of GLD patients, in which the diagnosis often follows the onset of symptoms. However, since the severe PNS damage, correction of CNS

lesion at this stage of disease progression was unlikely to improve the motor behavior and life span of Twi mice, which die mainly because of spastic paralysis and incapability to eat and breathe.

Multiple intracerebral vector injections are currently applied to increase the total number of transduced cells, in order to counterbalance limitation in transgene distribution and with the aim of approaching therapeutic levels of enzyme expression in the brain of non-human primates (9,26) and human patients (35,77). This greatly increases the invasiveness of the procedure, the total injected volume and the viral load in the brain. This, in turn, might trigger an inflammatory and immune response, also depending on the immunogenicity of the vector used (25,78). Using a single injection of 2×10^6TU bdLV in 1 μl, we achieved remarkable levels of enzymatic correction in the adult mouse brain (volume $\sim$0.5 cm^3) (79) without overt sign of neuroinflammation. Our results are in agreement with previous studies showing that brain parenchyma is an immunoprivileged site compared with the systemic or intrathecal/intraventricular compartment (78,80) and that maximal LV-mediated transgene expression with minimal increase of inflammation and immune response is achieved injecting between 10^6 and 10^7 TU in the rodent brain parenchyma (13,25,59).

The question remains as to whether this approach can be translated to larger brains. The most severe forms of leukodystrophies require neonatal intervention in order to obtain at least partial therapeutic efficacy (81). Improvements of technical and clinical tools currently allow precise deposition of considerable volumes of viral vector suspension at the site of interest, imparting considerable specificity and safety to the procedure (26,82,83). Still, safety issues might rise consequently to the increase in injected volume and viral load required to correct a $<$1 year human brain (volume $\sim$700 cm^3). Given the striking results described in our study, injection of $<$1 ml could be enough to reach therapeutic levels of enzyme correction. This would also address another potential limitation underlying the future clinical application of LV-based gene therapy, which is the relatively low yield currently achieved in large-scale LV production (84–86). Dose–response and biodistribution studies in non-human primates are now required to address these issues.

CONCLUSIONS

An intracerebral gene therapy approach achieving therapeutic benefit with limited or absent side effects relies on the proper combination of vector choice, dosing, target region and on deep knowledge of the molecular and biochemical properties of the transgene product. The intraparenchymal route of LV administration described in this work is effective in restoring the biological function of missing GALC and ARSA in the brain. The rapidly established long-term expression of enzyme with low dose and its remarkable diffusion from the transduced tissue warrant further consideration of this approach, which may provide a much needed benefit to patients of GLD, MLD and other devastating neurodegenerative LSD. Treatment performed in the asymptomatic stages and a combinatorial strategy ensuring rapid and long-term enzyme supply in the CNS (this approach) and in the PNS/periphery (i.e. ERT or HSCT) will likely succeed in preventing or substantially limiting the progression of these complex neurologic diseases.

MATERIALS AND METHODS

Animals

Twi mice bear a spontaneous point mutation resulting in a premature stop codon and no residual GALC activity (40,87). We used Twi mice on the mixed background of C57BL/6J and FVB (from hereon called Twi), which show a slower progressive form of GLD than the canonical Twi mice. Tremors develop at around PND21 and progress to severe resting tremor, weight loss, paralysis and wasting of hind legs. At 40 days, severe PNS and CNS demyelination is observed. Death occurs at around 45 days. The Twi mouse colony was maintained in the animal facility of the Fondazione San Raffaele del Monte Tabor, Milano, Italy. All procedures were performed according to protocols approved by an internal Animal Care and Use Committee (IACUC 325 and 314) and were reported to the Ministry of Health, as per Italian law. Homozygous Twi mice ($-/-$) and wild type ($+/+$) controls were obtained by strict brother–sister mating of heterozygous animals, and the genotyping of newborn mice was determined by polymerase chain reaction specific for the Twi mutation (88).

ARSA knockout mice ($As2^{-/-}$ or MLD mice) were generated by targeted disruption of the ARSA gene (46). $As2^{-/-}$ mice cannot metabolize sulfatides and, starting at 6–7 months, develop typical storage lesions, particularly in the fimbria and corpus callosum and, to a lower extent, in the PNS. At the same age, these mice also develop learning impairments that can be assessed by specific behavioral tests. However, these mice do not show the severity of symptoms observed in MLD human patients and have a normal life expectancy. $As2^{-/-}$ mice were bred by intercrossing the homozygous offspring of two carrier mice obtained by re-derivation (embryo transfer) of $As2^{-/-}$ males with C57BL/6 females. Thus, the MLD mice used in this study have a mixed C57BL6/129 genetic background. WT C57BL6/129 hybrid mice were purchased from The Jackson Laboratory and used as controls.

Vector production and titration

We used optimized bdLV allowing the coordinate expression of two transgenes driven by the human phosphoglycerate kinase (PGK) promoter (36): the CTRL vector encodes for two reporter genes (GFP and the truncated form of the low-affinity nerve growth factor receptor; *bdLV.ΔNGFR.GFP*). The therapeutic vectors were generated by replacing the ΔLNGFR cDNA of the CTRL vector with the murine GALC or ARSA cDNA C-terminally tagged with the human influenza hemagglutinin epitope (HA) (*bdLV.enzyme-HA.GFP*). Monocistronic PGK.GFP, PGK.GALC and PGK.ARSA LV (64) were used as control vectors. Reagents, detailed cloning procedures and sequence information are available upon request.

VSV-pseudotyped third-generation LV were produced by transient four-plasmid co-transfection into 293T cells and purified by ultracentrifugation as described (36), with the

modification that 1 mM sodium butyrate was added to the cultures for vector collection. Expression titer of GFP or ΔLNGFR vectors was estimated on HeLa cells by limiting dilution. Vector particle was measured by HIV-1 gag p24 antigen immunocapture (NEN Life Science Products). Vector infectivity was calculated as the ratio between titer and particle for the vector expressing GFP or ΔLNGFR. Titer of concentrated vector was $2–3 \times 10^9$ TU/ml and infectivity was $2–6 \times 10^4$ TU/ng of p24 for both bdLV.

NSC cultures

Neonatal (PND2) Twi mice, PND30 MLD mice and WT littermates were anaesthetized before being decapitated (using crushed ice and Avertin for neonates and adult mice, respectively). Brains were removed and the tissue containing the SVZ of the forebrain lateral ventricles was dissected. Tissues from three mice were pooled to establish a culture ($n = 3$ independent cultures). NSC cultures were established and expanded as described previously (39). For all the experiments, we used serially passaged NSC (passage 5th–15th). Differentiation of NSC was performed as described previously (39,89). Briefly, serially passaged 5-day-old neurospheres were dissociated and grown for 24 h in serum-free medium (DMEM/F12 1:1 vol:vol containing insulin, apo-transferrin, putrescine and progesterone) containing FGF2 and EGF (growth medium), in order to obtain a population enriched in proliferating, undifferentiated cells (precursor cells). This population was plated in the presence of an adhesion substrate, in serum-free medium containing FGF2. These cultures, which contained glial and neuronal progenitors at different stages of commitment, were exposed to serum-free medium containing 2% FCS and grown for additional 7 days, in order to achieve differentiation of neural progenitors into neurons, astrocytes and oligodendrocytes (differentiated cells). The extent of neuronal and glial differentiation/maturation in the different cell populations was assessed by using antibodies against lineage- and stage-specific markers, as described (39).

LV-mediated gene transfer in precursors and differentiated NSC

Precursor cells were incubated overnight with bdLV (3×10^7 TU/ml, MOI 100). BdLV-containing medium was then removed and neurospheres were subcultured every 5 days by mechanical dissociation. In this way, we established stable gene-corrected NSC lines that were further differentiated according to the protocol described earlier.

For transduction of differentiated cells, bdLV were added to the culture medium 1 day after NSC cultures have been shifted to serum-free medium containing 2% FCS. After an overnight incubation, bdLV-containing medium was then removed and fresh medium added. Cultures were grown for additional 5 days and then processed for different assays.

We evaluated the efficacy of transduction on the different gene-corrected NSC-derived cultures by quantifying (i) the number of HA- or GFP-expressing cells by immunohistochemistry and by FACS; (ii) VCN by qPCR; (iii) the presence of LV-encoded mRNA by RT–PCR; (iv) enzymatic activity by specific biochemical assays (43,90). The same analysis was performed in WT cells as well as in non-transduced and in cells transduced with the CTRL vectors. The effect of bdLV transduction on NSC functional features (survival, proliferation and differentiation capacity) was evaluated as described previously (39). Apoptosis was evaluated on differentiated NSC cultures by Caspase-3 staining and TUNEL assay (*In Situ* Cell Death Detection Kit, Roche).

Evaluation of cross-correction in NSC cultures

WT UT or gene-corrected Twi NSC are differentiated as described earlier and used as the source of secreted enzyme (donor cells). Twi NSC cultures (recipient cells), at the same stage of differentiation as donor cells, are exposed to the supernatant conditioned by differentiated donor cells during the last 72 h of culture. After a 24 h washout with fresh medium, donor cells, recipient cells and their supernatants are collected and analyzed for GALC activity.

LV injection

Twi and As2$^{-/-}$ mice (and WT littermates) were injected with bdLV at 3 weeks (PND 21) and 6 months of age, respectively, and were euthanized 3 weeks after injection.

Mice were anesthetized with Avertin (1.25 g of 2,2,2-tribromoethanol 99% + 2.5 ml of 2-methyl-2-buthanol 99% (Sigma-Aldrich) per 100 ml total volume; 110 μl/10g of body weight). A hole was drilled in the skull, and bdLV (1 μl; 2×10^6 total TU) were slowly injected in the left hemisphere by means of a 33G needle-Hamilton syringe (0.2 μl/min). The needle was left in place for additional 3 min and then slowly withdrawn. Stereotactic coordinates for the EC (mm from bregma, according to the Paxinos mouse brain atlas) were: AP 1.4, ML 2.5, DV −3. After the injection, the skull was carefully rinsed with ethanol, sutured and an antibiotic ointment was applied. Mice were then placed on a heating pad and monitored post-operatory. Mice were euthanized at PND42. A group of untreated Twi, As2$^{-/-}$ mice and WT littermates were included as controls. Details on the experimental groups are available in Supplementary Material, Table S1.

Tissue collection and processing

A group of mice were killed by CO_2 exposure and decapitated. Brain and spinal cord were isolated and either quickly frozen in liquid nitrogen or immediately processed to obtain tissue extracts. For biochemical and molecular assays, the two brain hemispheres were separated and cut in five rostro-caudal tissue slices including the areas of interest: (i) OB; (ii) anterior telencephalon (aTel), including the injected region; (iii) posterior telencephalon (pTel); (iv) cerebellum (Cb); (v) pons/medulla (Pons); (vi) total spinal cord (SC; cervical + thoracic + lumbar). In a subgroup of mice, we collected the CSF from the cysterna magna using a glass capillary immediately prior to euthanasia.

A second group of mice were intracardially perfused via the descending aorta (under deep anesthesia) with 0.9% NaCl followed by 4% paraformaldehyde in PBS. Brains and spinal cord tissues were collected and equilibrated for 24 h in 30%

sucrose in PBS and then included in 4% agarose. Serial coronal vibratome-cut sections (six series, 40 μm thick) were processed for histology and immunofluorescence analysis as described in what follows.

Immunohistochemistry

Cell cultures. Immunofluorescence was performed as previously described (39). We analyzed two to four replicates for each antigen in two to three independent experiments. Data are expressed as percentages of cells displaying immunoreactivity for each specific antigen (number of immunoreactive cells/total number of cells × 100). No detectable signal was observed in samples in which the primary antibodies were omitted.

Tissues. Free-floating vibratome-cut sections were incubated with blocking solution (10% normal goat serum + 0.3% Triton X-100 in PBS) for 1 h at RT and then incubated overnight at 4°C with primary antibody diluted in blocking solution. After thorough washing (three times 5 min each), antibody staining was revealed using species-specific fluorophore-conjugated secondary antibodies diluted in 10% normal goat serum + 0.1% Triton X-100 in PBS. Primary antibodies were mouse monoclonal anti-β-tubulin III (Babco, 1:2000), mouse anti-GalCer (1:300; MAB 342, Chemicon International), mouse anti-GFAP (1:1000; MAB3402, Chemicon International), mouse anti-HA (1:100; MMS-101P, Covance), mouse anti-NeuN (1:500; MAB377, Chemicon International), mouse anti-pan-NF (1:300; SMI 311, Sternberger Monoclonals); rat anti-MBP (1:300; MAB386, Chemicon International). rat anti-F4/80 (1:100; MCA4977, Serotec), rabbit anti-Iba1 (1:200; 019-19741, Wako), rabbit anti-Lamp-1 (1:200; AB 24170, Abcam), rabbit anti-GFAP (1:1000; ZO334, Dako, Denmark), chicken anti-GFP (1:1000; AB-13970, Abcam); rabbit anti-GST-π (1:500; 312, MBL), rabbit anti-GFP (1:1000; A-11122, Molecular Probes), chicken anti-GALC (CL1021AP, 1:10 000; a gift of Dr C.W. Lee), rabbit anti-NG2 (1:200; AB5320, Chemicon International), rabbit anti-cleaved Caspase-3 (Cell Signaling, 1:200).

Secondary antibodies were Alexa 488-, Alexa 546-, Alexa 633- (Molecular Probes), Cy3 (Jackson Lab)-conjugated anti-rabbit, anti-mouse, anti-rat, anti-chicken antibodies (1:1000).

Coverslips and tissue sections were counterstained with DAPI (10236276001, Roche) or ToPro-3 (T3605, Invitrogen), washed in PBS, collected and mounted on glass slides using Fluorsave (345789, CALBIOCHEM).

In vivo cell counts

The cell type composition of the transduced and/or cross-corrected cell population was assessed in matched coronal brain sections (two to four slices/mice; $n = 3$ mice/treatment group) selected within the region containing transduced (GFP^+) cells using anti-GFP and anti-GALC antibodies in combination with lineage-specific markers (NeuN for neurons; GFAP for astroglia; GST-π for oligodendroglia) and nuclear counterstaining (DAPI) in immunofluorescence followed by confocal microscopy analysis. To determine the percentage and the nature of transduced cells, triple-labeled sections were scanned with the confocal laser microscope, and a representative sample of 500–1000 transduced (GFP^+) and HA^+ cells (based on DAPI staining) was examined for co-localization with either lineage-specific marker. Results were expressed as: (i) the percentage GFP^+ cells/total number of nuclei (efficiency of transduction); (ii) the percentage of lineage $marker^+$ cells within the GFP^+ (transduced) cells; (iii) the percentage of lineage $marker^+$ cells within the HA^+ (both GFP^+ and GFP^-) cells.

Image acquisition

Samples (cell cultures and tissues) were visualized with (i) Zeiss Axioskop2 microscope using double-laser confocal microscopy with Zeiss Plan-Neofluar objective lens (Zeiss, Arese, Italy). Images were acquired using a Radiance 2100 camera (Bio-Rad, Segrate, Italy) and LaserSharp 2000 acquisition software (Bio-Rad); (ii) PerkinElmer UltraVIEW ERS Spinning Disk Confocal (PerkinElmer Life Sciences, Inc., MA, USA).

Z-stacks. Co-labeling between GFP and differentiation markers (GFAP, NeuN, GST-π, MBP, pan-NF) was analyzed in vibratome-cut tissue slides. Z-stacks were recorded utilizing a PerkinElmer UltraVIEW ERS Spinning Disk Confocal (PerkinElmer Life Sciences, Inc.) using a ×63/NA1.4 Planapochromat oil-immersion lens (Carl Zeiss, Jena, Germany) with a 405 nm diode laser, 488 nm argon laser and a 568 nm krypton laser excitation wavelengths. Sequential confocal images were collected at 0.25 μm intervals covering 14 μm depth (56 total scanning images for each channel). The 3D signals and the orthogonal projection representations were obtained by means of Volocity Software (v5.2.1; PerkinElmer-Improvision, Lexington, MA, USA). Images were imported into Adobe Photoshop CS3 (USA) and adjusted for brightness and contrast.

3D reconstruction and quantification of the bd.LV-transduced brain tissue were performed using a Leica DM 4000B microscope attached to a Neurolucida computer-assisted tracing system (Microbrightfield, Inc.,USA). For the calculation of GFP-transduced volume, every GFP^+ area on serial coronal sections (40 μm thick, 240 μm interval; $n = 12$ sections from one series, collected from the bregma −2 to 1 mm) was marked and attached to the subsequent trace according to the software instructions, as described previously (41).

Detection of storage

Lectin histochemistry was performed on vibratome-cut tissue slices. Slices were fixed for 10 min in 3% H_2O_2 in methanol; after washing in PBS (three times 5 min each), we applied a blocking kit (SP-2001, Vector Laboratories), followed by avidin solution (15 min) and biotin solution (15 min). Slides were subsequently incubated for 30 min with blocking solution (PBS: 0.3% Triton 10% NGS) and then with Biotinylated Ricinus Communis Agglutinin I (RCA I, B-1085 Vector Laboratories; 1:200 in blocking solution) for 30 min. After thorough washing (three times 5 min) and one passage in Tris–HCl (100 mM, 5 min), staining was revealed using VECTASTAIN ABC kit (PK-6100, Vector Laboratories).

After washings in Tris–HCl (100 mM, three times 5 min), reaction with the substrate 3,3′-diamino-benzidine tetrahydrochloride (DAB, 167 μg/ml in Tris–HCl 100 mM + H_2O_2 1:3000) was performed. Samples were visualized with a Nikon Eclipse E600 microscope. Images were acquired using a Nikon DMX 1200 digital camera and ACT-1 acquisition software (Nikon).

Detection of LV genome

Genomic DNA was extracted from whole-brain tissue (200600, DNA Extraction Kit, Stratagene) and quantified at NanoDrop ND-1000 Spectrophotometer (Euroclone, Pero, Italy). VCN were quantified by TaqMan analysis starting from 100 ng of template DNA extracted from the total brain tissue. Quantitative PCR was performed by amplifying the PSI sequence of the LV backbone using primers as follows: forward, 5′-TGAAAGCGA AAGGGAAACCA-3′; reverse, 5′-CCGTGCGCGCTTCAG-3′. PCR product length was 64 bp at a final concentration of 750 nmol for forward and 200 nmol for reverse primers. The probe was 5′-VIC-AGCTCTCTCGACGCAGGACTCGGC-MGB-3′ at a 200 nmol final concentration. As internal reference for normalization, we amplified a fragment of the murine β-actin gene using the following set of primers and probe: forward primer, 5′-AGAGGGAAATCGTGCGTGAC-3′ at 300 nmol final concentration; reverse primer, 5′-CAATAGTG ATGACCTGGCCGT-3′ at 750 nmol final concentration; the probe was 5′-VIC-CACTGCCGCATCCTCTTCCTCCCMG B-3′ at 200 nmol final concentration. A standard curve of genomic DNA carrying five LV copies, validated by Southern blot analysis, was constructed using DNA extracted from transgenic mouse tissue. The standard curve, based on different dilutions of DNA (from 200 to 25 ng) and, accordingly, of LV copies was used as standard both for LV and for β-actin amplification. Reactions were carried out in a total volume of 25 μl in an ABI Prism 7900 HT Sequence Detection System (Applied Biosystems). The VCN was calculated as follows: (ng LV/ng endogenous DNA) × (number of LV integrations in the standard curve).

Detection of GALC and GFP mRNA by RT–PCR

Total RNA was isolated from cells and tissues using TRIzol reagent (Invitrogen)/chloroform method and purified by RNeasy Mini Kit (Qiagen, Hilden, Germany). The quantity of RNA was determined by 260/280 nm optical density reading on a NanoDrop ND-1000 Spectrophotometer (NanoDrop, Pero, Italy). Reverse transcription was carried out using 1 μg of total RNA in the presence of 200 U of Quantitect Reverse Transcriptase kit (Qiagen, Hilden, Germany). PCR was carried out using *Taq* DNA polymerase (Qiagen) according to the manufacturer's protocol. Galc endogenous mRNA was amplified using forward and reverse primers into the mouse gene sequence (NM_008079), whereas for the transgenic one, we designed a reverse primer into the vector construct WPRE sequence (forward Galc: 5′-GAC TGT GCA GTG CGA TGT TT-3′; reverse Galc: 5′-GCC CTG AAC CAA AAT CAA AA-3′; reverse WPRE: 5′-AAG CCA TAC GGG AAG CAA TA-3′; annealing at 56°C). The endogenous product was 437 bp, and the transgenic product was 550 bp.

Gfp mRNA was amplified using the following forward and reverse primers: GFP forward: 5′-ACCCCGACCACATGAA GCAGC-3′; GFP reverse: 5′-CGTTGGGGTCTTTGCTCA GGG-3′ at 68°C. PCR product was 400 bp. All cDNAs used as templates were previously normalized throughout β-actin RT–PCR. The PCR products were separated on a 2% agarose gel at 10 V/cm and visualized by ethidium bromide.

Brain and cell extracts

Tissues were homogenized with an Elveheim-type homogenizer in 10 mmol/l sodium phosphate buffer, pH 6.0 (100 g/l) with 0.1% (vol/vol) Nonidet NP40 and then subjected to three rounds of sonication. After 1 h, brain lysates were centrifuged (12 000*g*) in Eppendorf microfuges for 15 min. We used supernatants as tissue extracts for biochemical analyses. All procedures were carried out at 4°C. Cells were harvested, washed in PBS, lysed for 1 h in 10 mmol/l sodium phosphate buffer, pH 6.0, containing 0.1% (vol/vol) Nonidet NP-40, and subjected to sonication. These steps were performed at 4°C. We measured protein content using the Bradford Protein Assay kit with bovine serum albumin as the reference standard.

WB analysis

After boiling for 5 min in sample buffer, samples containing 100 μg protein were separated through a 10% acrylamide gel SDS–PAGE electrophoresis.

The PDVF membranes were stained with chicken polyclonal anti-GALC antibody (1:2000; expected MW: 50 and 80 kDa); mouse monoclonal anti-GFP antibody (1:1000; A11121, Invitrogen; expected MW: 30 kDa) and goat polyclonal IgG anti-actin antibody (1:10 000; I-19, Santa Cruz Biotechnology; expected MW: 46 kDa), revealed by HRP-conjugated goat anti-mouse (1 20 000; AP124P, Chemicon), donkey anti-chicken (1:5000; SC-2953, Santa Cruz), rabbit anti-goat (1:40 000; AP132P, Chemicon) and incubated with chemiluminescent substrate Amersham ECL Plus™ kit (GE Healthcare).

Densitometry of WB bands. The 50 and 80 KDa bands revealed using the anti-GALC antibody were quantified by means of ImageJ software and the values (in pixels) obtained were normalized on those of the corresponding actin bands. Actin-normalized values were then expressed as the percentage of values obtained from region-matched bands of WT tissues according to the formula: (pixel GALC/pixel β-actin) × 100/pixel WT.

For immunomagnetic pull down of HA-tagged protein, samples (300 μg total protein extracts) were incubated with anti-HA microbeads (μMACS HA Tagged Protein Isolation Kit, 130-091-122, Miltenyi Biotec) and then passed through μ Columns (130-042-701, Miltenyi Biotec) in Multistand-μMACS Separator strong magnetic field. The HA-enriched lysates was then processed for WB using a mouse HRP-conjugated anti-HA antibody (1:2000; 120-002.341, Miltenyi Biotec).

Determination of enzyme activity

GALC activity is measured using a recently developed assay (44). We performed the assay using 2–7.5 μg of sample proteins with the artificial fluorogenic substrate 4-methylumbelliferone-β-galactopyranoside (1.5 mM) resuspended in 0.1/0.2 mol/l citrate/phosphate buffer, pH 4.0, and AgNO3 (11 mM) at 37°C.

ARSA activity was determined using the 4-methylumbelliferyl-sulfate substrate dissolved in 0.05 M Na-acetate/acetic acid buffer, pH 5.5, in the presence or absence of 125 mM $AgNO_3$ (a specific ARSA inhibitor) at 37°C (90). ARSA activity was calculated by subtracting the value obtained in the presence of $AgNO_3$ (arylsulfatase B – ARSB activity) from that measured in the absence of the inhibitor (ARSA + ARSB activity).

All enzymatic reactions were stopped by adding 0.2 M glycine/NaOH, pH 10.6. Fluorescence of liberated 4-ethylumbelliferone was measured on a spectrofluorometer (λ_{ex} 360 nm; λ_{em} 446 nm).

Sephadex S-300 gel filtration

One microgram of proteins from WT or Twi brain tissues extracts was loaded onto a Sephadex S-300 gel filtration column (1 $cm^2 \times 48$ cm), previously equilibrated with 10 mmol/l sodium phosphate buffer, pH 6.0, and run in the same buffer at a flow rate of 0.1 ml/min. Molecular masses were evaluated using the following standards: Dextran blue (2000 kDa); apoferritin (443 kDa), B-amilase (200 kDa), alcohol dehydrogenase (150 kDa), bovine serum albumin (66 kDa), carbonic anhydrase (29 kDa). The procedure was carried out at 4°C. Fractions (0.4 ml) were collected and analyzed for GALC enzyme activity.

Statistics

In vitro and *in vivo* cell counts, enzyme activity, VCN values and data obtained following the quantification of immunopositive area by the ImageJ software were analyzed with GraphPad Prism version 5.0a for Macintosh and expressed as the mean ± SE. Unpaired Student's *t*-test or two-way ANOVA followed by Bonferroni post-tests (statistical significance $P < 0.05$) was used when appropriate. The number of samples analyzed and the statistical test applied are indicated in the legends to each figure.

SUPPLEMENTARY MATERIAL

Supplementary Material is available at *HMG* online.

ACKNOWLEDGEMENTS

We thank Chris W. Lee (Mayo Clinic College of Medicine, Jacksonville, FL, USA) for kindly providing the CL1021AP antibody. We acknowledge the technical help of Daniele Conti Roberto Tiribuzi and Eugenia Barone (University of Perugia, Italy) for the analysis of GALC activity and gel filtration chromatography; Lucia Sergi Sergi (HSR-TIGET) for bdLV.CTRL and bdLV.GALC production; Francesca Ruffini (CSF collection), Melania Cusimano and Stefano Pluchino (help with Neurolucida Software) (Institute of Experimental Neurology, San Raffaele Scientific Institute). Cesare Covino (Advanced Light and Electron Microscopy BioImaging Center, ALEMBIC, San Raffaele Scientific Institute) for image acquisition and analysis. The bdLV.ARSA was kindly provided by Alessia Capotondo (HSR-TIGET). We are grateful to all members in A.G.'s laboratory, in particular to Chiara Cavazzin for NSC *in vitro* transduction with LV.ARSA. We thank Alessandra Biffi and Ilaria Visigalli (HSR-TIGET) for their helpful suggestions and for critical discussion of results.

Conflict of interest: none declared.

FUNDING

This work was supported by grants from the Italian Telethon Foundation (TIGET grants to A.G.-TGT06B02-, and L.N.), the European Leukodystrophy Association (ELA; grant 2008-027I5 to A.G.), the Italian Ministry of Health (ex art. 56L 289/2002 to A.G. and L.N.).

REFERENCES

1. Vellodi, A. (2005) Lysosomal storage disorders. *Br. J. Haematol*, **128**, 413–431.
2. Suzuki, K. and Suzuki, Y. (1970) Globoid cell leucodystrophy (Krabbe's disease): deficiency of galactocerebroside beta-galactosidase. *Proc. Natl Acad. Sci. USA*, **66**, 302–309.
3. Gieselmann, V., Kreysing, J. and von Figura, K. (1994) Genetics of metachromatic leukodystrophy. *Gene Ther.*, **1** (Suppl. 1), S87.
4. Sands, M.S. and Haskins, M.E. (2008) CNS-directed gene therapy for lysosomal storage diseases. *Acta. Paediatr. Suppl.*, **97**, 22–27.
5. Broekman, M.L., Baek, R.C., Comer, L.A., Fernandez, J.L., Seyfried, T.N. and Sena-Esteves, M. (2007) Complete correction of enzymatic deficiency and neurochemistry in the GM1-gangliosidosis mouse brain by neonatal adeno-associated virus-mediated gene delivery. *Mol. Ther.*, **15**, 30–37.
6. Broekman, M.L., Tierney, L.A., Benn, C., Chawla, P., Cha, J.H. and Sena-Esteves, M. (2009) Mechanisms of distribution of mouse beta-galactosidase in the adult GM1-gangliosidosis brain. *Gene Ther.*, **16**, 303–308.
7. Cachon-Gonzalez, M.B., Wang, S.Z., Lynch, A., Ziegler, R., Cheng, S.H. and Cox, T.M. (2006) Effective gene therapy in an authentic model of Tay-Sachs-related diseases. *Proc. Natl Acad. Sci. USA*, **103**, 10373–10378.
8. Martino, S., Marconi, P., Tancini, B., Dolcetta, D., De Angelis, M.G., Montanucci, P., Bregola, G., Sandhoff, K., Bordignon, C., Emiliani, C. *et al.* (2005) A direct gene transfer strategy via brain internal capsule reverses the biochemical defect in Tay-Sachs disease. *Hum. Mol. Genet.*, **14**, 2113–2123.
9. Vite, C.H., McGowan, J.C., Niogi, S.N., Passini, M.A., Drobatz, K.J., Haskins, M.E. and Wolfe, J.H. (2005) Effective gene therapy for an inherited CNS disease in a large animal model. *Ann. Neurol.*, **57**, 355–364.
10. Cearley, C.N. and Wolfe, J.H. (2007) A single injection of an adeno-associated virus vector into nuclei with divergent connections results in widespread vector distribution in the brain and global correction of a neurogenetic disease. *J. Neurosci.*, **27**, 9928–9940.
11. Liu, G., Chen, Y.H., He, X., Martins, I., Heth, J.A., Chiorini, J.A. and Davidson, B.L. (2007) Adeno-associated virus type 5 reduces learning deficits and restores glutamate receptor subunit levels in MPS VII mice CNS. *Mol. Ther.*, **15**, 242–247.
12. Di Domenico, C., Villani, G.R., Di Napoli, D., Nusco, E., Cali, G., Nitsch, L. and Di Natale, P. (2009) Intracranial gene delivery of LV-NAGLU vector corrects neuropathology in murine MPS IIIB. *Am. J. Med. Genet.*, **149A**, 1209–1218.
13. Di Natale, P., Di Domenico, C., Gargiulo, N., Castaldo, S., Gonzalez, Y.R.E., Mithbaokar, P., De Felice, M., Follenzi, A., Naldini, L. and Villani,

G.R. (2005) Treatment of the mouse model of mucopolysaccharidosis type IIIB with lentiviral-NAGLU vector. *Biochem. J.*, **388**, 639–646.
14. Cabrera-Salazar, M.A., Roskelley, E.M., Bu, J., Hodges, B.L., Yew, N., Dodge, J.C., Shihabuddin, L.S., Sohar, I., Sleat, D.E., Scheule, R.K. *et al.* (2007) Timing of therapeutic intervention determines functional and survival outcomes in a mouse model of late infantile batten disease. *Mol. Ther.*, **15**, 1782–1788.
15. Passini, M.A., Macauley, S.L., Huff, M.R., Taksir, T.V., Bu, J., Wu, I.H., Piepenhagen, P.A., Dodge, J.C., Shihabuddin, L.S., O'Riordan, C.R. *et al.* (2005) AAV vector-mediated correction of brain pathology in a mouse model of Niemann–Pick A disease. *Mol. Ther.*, **11**, 754–762.
16. Sevin, C., Benraiss, A., Van Dam, D., Bonnin, D., Nagels, G., Verot, L., Laurendeau, I., Vidaud, M., Gieselmann, V., Vanier, M. *et al.* (2006) Intracerebral adeno-associated virus-mediated gene transfer in rapidly progressive forms of metachromatic leukodystrophy. *Hum. Mol. Genet.*, **15**, 53–64.
17. Consiglio, A., Quattrini, A., Martino, S., Bensadoun, J.C., Dolcetta, D., Trojani, A., Benaglia, G., Marchesini, S., Cestari, V., Oliverio, A. *et al.* (2001) *In vivo* gene therapy of metachromatic leukodystrophy by lentiviral vectors: correction of neuropathology and protection against learning impairments in affected mice. *Nat. Med.*, **7**, 310–316.
18. Rafi, M.A., Zhi Rao, H., Passini, M.A., Curtis, M., Vanier, M.T., Zaka, M., Luzi, P., Wolfe, J.H. and Wenger, D.A. (2005) AAV-mediated expression of galactocerebrosidase in brain results in attenuated symptoms and extended life span in murine models of globoid cell leukodystrophy. *Mol. Ther.*, **11**, 734–744.
19. Lin, D., Fantz, C.R., Levy, B., Rafi, M.A., Vogler, C., Wenger, D.A. and Sands, M.S. (2005) AAV2/5 vector expressing galactocerebrosidase ameliorates CNS disease in the murine model of globoid-cell leukodystrophy more efficiently than AAV2. *Mol. Ther.*, **12**, 422–430.
20. Colle, M.A., Piguet, F., Bertrand, L., Raoul, S., Bieche, I., Dubreil, L., Sloothaak, D., Bouquet, C., Moullier, P., Aubourg, P. *et al.* (2009) Efficient intracerebral delivery of Aav5 vector encoding human Arsa in non-human primate. *Hum. Mol. Genet.*, **19**, 147–158.
21. McCown, T.J. (2005) Adeno-associated virus (AAV) vectors in the CNS. *Curr. Gene Ther.*, **5**, 333–338.
22. Passini, M.A., Watson, D.J. and Wolfe, J.H. (2004) Gene delivery to the mouse brain with adeno-associated virus. *Methods Mol. Biol.*, **246**, 225–236.
23. Deglon, N. and Aebischer, P. (2002) Lentiviruses as vectors for CNS diseases. *Curr. Top. Microbiol. Immunol.*, **261**, 191–209.
24. Lundberg, C., Bjorklund, T., Carlsson, T., Jakobsson, J., Hantraye, P., Deglon, N. and Kirik, D. (2008) Applications of lentiviral vectors for biology and gene therapy of neurological disorders. *Curr. Gene Ther.*, **8**, 461–473.
25. Abordo-Adesida, E., Follenzi, A., Barcia, C., Sciascia, S., Castro, M.G., Naldini, L. and Lowenstein, P.R. (2005) Stability of lentiviral vector-mediated transgene expression in the brain in the presence of systemic antivector immune responses. *Hum. Gene Ther.*, **16**, 741–751.
26. Hadaczek, P., Forsayeth, J., Mirek, H., Munson, K., Bringas, J., Pivirotto, P., McBride, J.L., Davidson, B.L. and Bankiewicz, K.S. (2009) Transduction of nonhuman primate brain with adeno-associated virus serotype 1: vector trafficking and immune response. *Hum. Gene Ther.*, **20**, 225–237.
27. Wong, L.F., Goodhead, L., Prat, C., Mitrophanous, K.A., Kingsman, S.M. and Mazarakis, N.D. (2006) Lentivirus-mediated gene transfer to the central nervous system: therapeutic and research applications. *Hum. Gene Ther.*, **17**, 1–9.
28. Schambach, A. and Baum, C. (2008) Clinical application of lentiviral vectors - concepts and practice. *Curr. Gene Ther*, **8**, 474–482.
29. Montini, E., Cesana, D., Schmidt, M., Sanvito, F., Bartholomae, C.C., Ranzani, M., Benedicenti, F., Sergi, L.S., Ambrosi, A., Ponzoni, M. *et al.* (2009) The genotoxic potential of retroviral vectors is strongly modulated by vector design and integration site selection in a mouse model of HSC gene therapy. *J. Clin. Invest.*, **119**, 964–975.
30. Passini, M.A., Lee, E.B., Heuer, G.G. and Wolfe, J.H. (2002) Distribution of a lysosomal enzyme in the adult brain by axonal transport and by cells of the rostral migratory stream. *J. Neurosci.*, **22**, 6437–6446.
31. Biffi, A., De Palma, M., Quattrini, A., Del Carro, U., Amadio, S., Visigalli, I., Sessa, M., Fasano, S., Brambilla, R., Marchesini, S. *et al.* (2004) Correction of metachromatic leukodystrophy in the mouse model by transplantation of genetically modified hematopoietic stem cells. *J. Clin. Invest.*, **113**, 1118–1129.
32. Luca, T., Givogri, M.I., Perani, L., Galbiati, F., Follenzi, A., Naldini, L. and Bongarzone, E.R. (2005) Axons mediate the distribution of arylsulfatase A within the mouse hippocampus upon gene delivery. *Mol. Ther.*, **12**, 669–679.
33. Vite, C.H., Passini, M.A., Haskins, M.E. and Wolfe, J.H. (2003) Adeno-associated virus vector-mediated transduction in the cat brain. *Gene Ther.*, **10**, 1874–1881.
34. Ciron, C., Cressant, A., Roux, F., Raoul, S., Cherel, Y., Hantraye, P., Deglon, N., Schwartz, B., Barkats, M., Heard, J.M. *et al.* (2009) Human alpha-iduronidase gene transfer mediated by adeno-associated virus types 1, 2 and 5 in the brain of nonhuman primates: vector diffusion and biodistribution. *Hum. Gene Ther.*, **20**, 350–360.
35. Worgall, S., Sondhi, D., Hackett, N.R., Kosofsky, B., Kekatpure, M.V., Neyzi, N., Dyke, J.P., Ballon, D., Heier, L., Greenwald, B.M. *et al.* (2008) Treatment of late infantile neuronal ceroid lipofuscinosis by CNS administration of a serotype 2 adeno-associated virus expressing CLN2 cDNA. *Hum. Gene Ther.*, **19**, 463–474.
36. Amendola, M., Venneri, M.A., Biffi, A., Vigna, E. and Naldini, L. (2005) Coordinate dual-gene transgenesis by lentiviral vectors carrying synthetic bidirectional promoters. *Nat. Biotechnol.*, **23**, 108–116.
37. Duchen, L.W., Eicher, E.M., Jacobs, J.M., Scaravilli, F. and Teixeira, F. (1980) Hereditary leucodystrophy in the mouse: the new mutant twitcher. *Brain*, **103**, 695–710.
38. Suzuki, K. (1983) The twitcher mouse. A model of human globoid cell leukodystrophy (Krabbe's disease). *Am. J. Pathol.*, **111**, 394–397.
39. Gritti, A., Dal Molin, M., Foroni, C. and Bonfanti, L. (2009) Effects of developmental age, brain region, and time in culture on long-term proliferation and multipotency of neural stem cell populations. *J. Comp. Neurol.*, **517**, 333–349.
40. Lee, W.C., Tsoi, Y.K., Dickey, C.A., Delucia, M.W., Dickson, D.W. and Eckman, C.B. (2006) Suppression of galactosylceramidase (GALC) expression in the twitcher mouse model of globoid cell leukodystrophy (GLD) is caused by nonsense-mediated mRNA decay (NMD). *Neurobiol. Dis.*, **23**, 273–280.
41. Bacigaluppi, M., Pluchino, S., Peruzzotti Jametti, L., Kilic, E., Kilic, U., Salani, G., Brambilla, E., West, M.J., Comi, G., Martino, G. *et al.* (2009) Delayed post-ischaemic neuroprotection following systemic neural stem cell transplantation involves multiple mechanisms. *Brain*, **132**, 2239–2251.
42. Lee, W.C., Courtenay, A., Troendle, F.J., Stallings-Mann, M.L., Dickey, C.A., Delucia, M.W., Dickson, D.W. and Eckman, C.B. (2005) Enzyme replacement therapy results in substantial improvements in early clinical phenotype in a mouse model of globoid cell leukodystrophy. *FASEB J.*, **19**, 1549–1551.
43. Martino, S., Tiribuzi, R., Tortori, A., Conti, D., Visigalli, I., Lattanzi, A., Biffi, A., Gritti, A. and Orlacchio, A. (2009) Specific determination of beta-galactocerebrosidase activity via competitive inhibition of beta-galactosidase. *Clin. Chem.*, **55**, 541–548.
44. Nagano, S., Yamada, T., Shinnoh, N., Furuya, H., Taniwaki, T. and Kira, J. (1998) Expression and processing of recombinant human galactosylceramidase. *Clin. Chim. Acta.*, **276**, 53–61.
45. Ben-Yoseph, Y., Hungerford, M. and Nadler, H.L. (1980) The interrelations between high- and low-molecular weight forms of normal and mutant (Krabbe-disease) galactocerebrosidase. *Biochem. J.*, **189**, 9–15.
46. Hess, B., Saftig, P., Hartmann, D., Coenen, R., Lullmann-Rauch, R., Goebel, H.H., Evers, M., von Figura, K., D'Hooge, R., Nagels, G. *et al.* (1996) Phenotype of arylsulfatase A-deficient mice: relationship to human metachromatic leukodystrophy. *Proc. Natl Acad. Sci. USA*, **93**, 14821–14826.
47. Shen, J.S., Watabe, K., Ohashi, T. and Eto, Y. (2001) Intraventricular administration of recombinant adenovirus to neonatal twitcher mouse leads to clinicopathological improvements. *Gene Ther.*, **8**, 1081–1087.
48. Liu, G., Martins, I., Wemmie, J.A., Chiorini, J.A. and Davidson, B.L. (2005) Functional correction of CNS phenotypes in a lysosomal storage disease model using adeno-associated virus type 4 vectors. *J. Neurosci.*, **25**, 9321–9327.
49. Chang, M., Cooper, J.D., Sleat, D.E., Cheng, S.H., Dodge, J.C., Passini, M.A., Lobel, P. and Davidson, B.L. (2008) Intraventricular enzyme replacement improves disease phenotypes in a mouse model of late infantile neuronal ceroid lipofuscinosis. *Mol. Ther.*, **16**, 649–656.
50. Watson, G., Bastacky, J., Belichenko, P., Buddhikot, M., Jungles, S., Vellard, M., Mobley, W.C. and Kakkis, E. (2006) Intrathecal administration of AAV vectors for the treatment of lysosomal storage in the brains of MPS I mice. *Gene Ther.*, **13**, 917–925.

51. Passini, M.A., Watson, D.J., Vite, C.H., Landsburg, D.J., Feigenbaum, A.L. and Wolfe, J.H. (2003) Intraventricular brain injection of adeno-associated virus type 1 (AAV1) in neonatal mice results in complementary patterns of neuronal transduction to AAV2 and total long-term correction of storage lesions in the brains of beta-glucuronidase-deficient mice. *J. Virol.*, **77**, 7034–7040.
52. Eto, Y., Shen, J.S., Meng, X.L. and Ohashi, T. (2004) Treatment of lysosomal storage disorders: cell therapy and gene therapy. *J. Inherit. Metab. Dis.*, **27**, 411–415.
53. Alroy, J., Ucci, A.A., Goyal, V. and Aurilio, A. (1986) Histochemical similarities between human and animal globoid cells in Krabbe's disease: a lectin study. *Acta Neuropathol.*, **71**, 26–31.
54. Alroy, J., Ucci, A.A., Goyal, V. and Woods, W. (1986) Lectin histochemistry of glycolipid storage diseases on frozen and paraffin-embedded tissue sections. *J. Histochem. Cytochem.*, **34**, 501–505.
55. Dolcetta, D., Perani, L., Givogri, M.I., Galbiati, F., Amadio, S., Del Carro, U., Finocchiaro, G., Fanzani, A., Marchesini, S., Naldini, L. *et al.* (2006) Design and optimization of lentiviral vectors for transfer of GALC expression in twitcher brain. *J. Gene Med.*, **8**, 962–971.
56. Sandhu, J.K., Gardaneh, M., Iwasiow, R., Lanthier, P., Gangaraju, S., Ribecco-Lutkiewicz, M., Tremblay, R., Kiuchi, K. and Sikorska, M. (2009) Astrocyte-secreted GDNF and glutathione antioxidant system protect neurons against 6OHDA cytotoxicity. *Neurobiol. Dis.*, **33**, 405–414.
57. Desclaux, M., Teigell, M., Amar, L., Vogel, R., Gimenez, Y.R.M., Privat, A. and Mallet, J. (2009) A novel and efficient gene transfer strategy reduces glial reactivity and improves neuronal survival and axonal growth in vitro. *PLoS One*, **4**, e6227.
58. Blomer, U., Naldini, L., Kafri, T., Trono, D., Verma, I.M. and Gage, F.H. (1997) Highly efficient and sustained gene transfer in adult neurons with a lentivirus vector. *J. Virol.*, **71**, 6641–6649.
59. Alisky, J.M., Hughes, S.M. and Davidson, B.L. (2003) Transduction of neurons lining the cerebral external capsules in mice with feline immunodeficiency virus based vectors. *Neurosci. Lett.*, **351**, 120–124.
60. Kordower, J.H., Emborg, M.E., Bloch, J., Ma, S.Y., Chu, Y., Leventhal, L., McBride, J., Chen, E.Y., Palfi, S., Roitberg, B.Z. *et al.* (2000) Neurodegeneration prevented by lentiviral vector delivery of GDNF in primate models of Parkinson's disease. *Science*, **290**, 767–773.
61. Brooks, A.I., Stein, C.S., Hughes, S.M., Heth, J., McCray, P.M. Jr, Sauter, S.L., Johnston, J.C., Cory-Slechta, D.A., Federoff, H.J. and Davidson, B.L. (2002) Functional correction of established central nervous system deficits in an animal model of lysosomal storage disease with feline immunodeficiency virus-based vectors. *Proc. Natl Acad. Sci. USA*, **99**, 6216–6221.
62. Croci, C., Fasano, S., Superchi, D., Perani, L., Martellosio, A., Brambilla, R., Consalez, G. and Bongarzone, E.R. (2006) Cerebellar neurons and glial cells are transducible by lentiviral vectors without decrease of cerebellar functions. *Dev. Neurosci.*, **28**, 216–221.
63. McIver, S.R., Lee, C.S., Lee, J.M., Green, S.H., Sands, M.S., Snider, B.J. and Goldberg, M.P. (2005) Lentiviral transduction of murine oligodendrocytes *in vivo*. *J. Neurosci. Res.*, **82**, 397–403.
64. Consiglio, A., Gritti, A., Dolcetta, D., Follenzi, A., Bordignon, C., Gage, F.H., Vescovi, A.L. and Naldini, L. (2004) Robust *in vivo* gene transfer into adult mammalian neural stem cells by lentiviral vectors. *Proc. Natl Acad. Sci. USA*, **101**, 14835–14840.
65. Bosch, A., Perret, E., Desmaris, N., Trono, D. and Heard, J.M. (2000) Reversal of pathology in the entire brain of mucopolysaccharidosis type VII mice after lentivirus-mediated gene transfer. *Hum. Gene Ther.*, **11**, 1139–1150.
66. Krivit, W., Aubourg, P., Shapiro, E. and Peters, C. (1999) Bone marrow transplantation for globoid cell leukodystrophy, adrenoleukodystrophy, metachromatic leukodystrophy, and Hurler syndrome. *Curr. Opin. Hematol.*, **6**, 377–382.
67. Escolar, M.L., Poe, M.D., Smith, J.K., Gilmore, J.H., Kurtzberg, J., Lin, W. and Styner, M. (2009) Diffusion tensor imaging detects abnormalities in the corticospinal tracts of neonates with infantile Krabbe disease. *AJNR Am. J. Neuroradiol.*, **30**, 1017–1021.
68. Couce, M.E., Weatherington, A.J. and McGinty, J.F. (1992) Expression of insulin-like growth factor-II (IGF-II) and IGF-II/mannose-6-phosphate receptor in the rat hippocampus: an *in situ* hybridization and immunocytochemical study. *Endocrinology*, **131**, 1636–1642.
69. Hawkes, C. and Kar, S. (2003) Insulin-like growth factor-II/mannose-6-phosphate receptor: widespread distribution in neurons of the central nervous system including those expressing cholinergic phenotype. *J. Comp. Neurol.*, **458**, 113–127.
70. Hawkes, C. and Kar, S. (2004) The insulin-like growth factor-II/mannose-6-phosphate receptor: structure, distribution and function in the central nervous system. *Brain Res. Brain Res. Rev.*, **44**, 117–140.
71. Neufeld, E.F. (1991) Lysosomal storage diseases. *Annu. Rev. Biochem.*, **60**, 257–280.
72. Lee, W.C., Tsoi, Y.K., Troendle, F.J., DeLucia, M.W., Ahmed, Z., Dicky, C.A., Dickson, D.W. and Eckman, C.B. (2007) Single-dose intracerebroventricular administration of galactocerebrosidase improves survival in a mouse model of globoid cell leukodystrophy. *FASEB J.*, **21**, 2520–2527.
73. Chen, Y.Q. and Wenger, D.A. (1993) Galactocerebrosidase from human urine: purification and partial characterization. *Biochim. Biophys. Acta.*, **1170**, 53–61.
74. Fraldi, A., Biffi, A., Lombardi, A., Visigalli, I., Pepe, S., Settembre, C., Nusco, E., Auricchio, A., Naldini, L., Ballabio, A. *et al.* (2007) SUMF1 enhances sulfatase activities *in vivo* in five sulfatase deficiencies. *Biochem. J.*, **403**, 305–312.
75. Jeyakumar, M., Dwek, R.A., Butters, T.D. and Platt, F.M. (2005) Storage solutions: treating lysosomal disorders of the brain. *Nat. Rev. Neurosci.*, **6**, 713–725.
76. Jeyakumar, M., Lee, J.P., Sibson, N.R., Lowe, J.P., Stuckey, D.J., Tester, K., Fu, G., Newlin, R., Smith, D.A., Snyder, E.Y. *et al.* (2009) Neural stem cell transplantation benefits a monogenic neurometabolic disorder during the symptomatic phase of disease. *Stem Cells*, **27**, 2362–2370.
77. McPhee, S.W., Janson, C.G., Li, C., Samulski, R.J., Camp, A.S., Francis, J., Shera, D., Lioutermann, L., Feely, M., Freese, A. *et al.* (2006) Immune responses to AAV in a phase I study for Canavan disease. *J. Gene Med.*, **8**, 577–588.
78. Lowenstein, P.R., Mandel, R.J., Xiong, W.D., Kroeger, K. and Castro, M.G. (2007) Immune responses to adenovirus and adeno-associated vectors used for gene therapy of brain diseases: the role of immunological synapses in understanding the cell biology of neuroimmune interactions. *Curr. Gene Ther.*, **7**, 347–360.
79. Kooy, R.F., Reyniers, E., Verhoye, M., Sijbers, J., Bakker, C.E., Oostra, B.A., Willems, P.J. and Van Der Linden, A. (1999) Neuroanatomy of the fragile X knockout mouse brain studied using *in vivo* high resolution magnetic resonance imaging. *Eur. J. Hum. Genet.*, **7**, 526–532.
80. Lowenstein, P.R., Kroeger, K. and Castro, M.G. (2007) Immunology of neurological gene therapy: how T cells modulate viral vector-mediated therapeutic transgene expression through immunological synapses. *Neurotherapeutics*, **4**, 715–724.
81. Escolar, M.L., Poe, M.D., Provenzale, J.M., Richards, K.C., Allison, J., Wood, S., Wenger, D.A., Pietryga, D., Wall, D., Champagne, M. *et al.* (2005) Transplantation of umbilical-cord blood in babies with infantile Krabbe's disease. *N. Engl. J. Med.*, **352**, 2069–2081.
82. Hadaczek, P., Kohutnicka, M., Krauze, M.T., Bringas, J., Pivirotto, P., Cunningham, J. and Bankiewicz, K. (2006) Convection-enhanced delivery of adeno-associated virus type 2 (AAV2) into the striatum and transport of AAV2 within monkey brain. *Hum. Gene Ther.*, **17**, 291–302.
83. Kells, A.P., Hadaczek, P., Yin, D., Bringas, J., Varenika, V., Forsayeth, J. and Bankiewicz, K.S. (2009) Efficient gene therapy-based method for the delivery of therapeutics to primate cortex. *Proc. Natl Acad. Sci. USA*, **106**, 2407–2411.
84. Sena-Esteves, M., Tebbets, J.C., Steffens, S., Crombleholme, T. and Flake, A.W. (2004) Optimized large-scale production of high titer lentivirus vector pseudotypes. *J. Virol. Methods*, **122**, 131–139.
85. Bank, A., Dorazio, R. and Leboulch, P. (2005) A phase I/II clinical trial of beta-globin gene therapy for beta-thalassemia. *Ann. N. Y. Acad. Sci.*, **1054**, 308–316.
86. Cartier, N., Hacein-Bey-Abina, S., Bartholomae, C.C., Veres, G., Schmidt, M., Kutschera, I., Vidaud, M., Abel, U., Dal-Cortivo, L., Caccavelli, L. *et al.* (2009) Hematopoietic stem cell gene therapy with a lentiviral vector in X-linked adrenoleukodystrophy. *Science*, **326**, 818–823.
87. Suzuki, K. (1995) The twitcher mouse: a model for Krabbe disease and for experimental therapies. *Brain Pathol.*, **5**, 249–258.
88. Sakai, N., Inui, K., Tatsumi, N., Fukushima, H., Nishigaki, T., Taniike, M., Nishimoto, J., Tsukamoto, H., Yanagihara, I., Ozono, K. *et al.* (1996) Molecular cloning and expression of cDNA for murine galactocerebrosidase and mutation analysis of the twitcher mouse, a model of Krabbe's disease. *J. Neurochem.*, **66**, 1118–1124.

89. Martino, S., di Girolamo, I., Cavazzin, C., Tiribuzi, R., Galli, R., Rivaroli, A., Valsecchi, M., Sandhoff, K., Sonnino, S., Vescovi, A. *et al.* (2009) Neural precursor cell cultures from GM2-gangliosidosis animal models recapitulate the biochemical and molecular hallmarks of the brain pathology. *J. Neurochem.*, **109**, 135–147.

90. Martino, S., Consiglio, A., Cavalieri, C., Tiribuzi, R., Costanzi, E., Severini, G.M., Emiliani, C., Bordignon, C. and Orlacchio, A. (2005) Expression and purification of a human, soluble arylsulfatase A for metachromatic leukodystrophy enzyme replacement therapy. *J. Biotechnol.*, **117**, 243–251.